In: Porous Media
Editor: Doris Wolfe, pp. 1-52
ISBN: 978-1-63485-452-8

Chapter 1

HYBRID MODELING AND ANALYSIS OF MULTICOMPONENT ADSORPTION WITH APPLICATIONS TO COALBED METHANE*

F. P. Medina and M. Peszynska
Oregon State University, Department of Mathematics,
Corvallis, OR, US

Abstract

In this paper we consider non-standard models of multi-component adsorption with applications to gas adsorption processes in coalbeds. In particular we follow thermodynamically consistent approaches, both at macroscale, via the Ideal Adsorbate Solution (IAS) theory, as well as at the pore-scale (built with statistical mechanics and specifically with mean-field equilibrium approach). The models we consider do not have a simple algebraic form, and therefore their analyses and numerical simulation have challenges. We present several mathematical analysis results and numerical solutions to illustrate the issues.

*Research presented in this paper was partially supported by the grants NSF-DMS 1115827 "Hybrid modeling in porous media"and NSF-DMS 1522734 "Phase transitions in porous media across multiple scales".

1. Introduction

In this paper we consider non-standard models of multi-component adsorption with applications to gas adsorption processes in coalbeds.

Coalbeds have the form of coal seams surrounded by sandstone, gravel, mudstone or shales. The coal seams have a multiscale structure of microporous coal matrix interspersed with cleats i.e. fractures or macropores; see Figure 1. Coalbed methane is a form of natural gas extracted from coal beds, and coal and methane are an important energy resource exported from US. In the Enhanced Coalbed Methane (ECBM) technology, carbon dioxide and/or nitrogen or other gases are injected into unmineable coal seams to promote displacement and extraction of methane. Simultaneously, ECBM provides a possibility to store carbon dioxide, thus ECBM is a potential carbon sequestration technique; see, e.g. [76, 22, 81, 40, 73, 20, 19].

The modeling challenges include accounting for competitive or preferential adsorption [11, 12, 9, 68, 27, 25, 38]. Further, one should model the experimentally observed phenomena such as adsorption-desorption hysteresis [13, 66, 57] and coal matrix swelling [46, 12, 68, 83, 38, 74]. Attempts to fit the data to empirical relationships for these phenomena were described in [13, 8, 47, 39, 70, 14], and single-component hysteresis was modeled and analyzed in [50, 53].

In this paper we discuss hybrid models of multicomponent transport with adsorption involving the porescale in a thermodynamically consistent way. Even though we do not address hysteresis or coal matrix swelling here, these models can account for these complex phenomena in a natural way. In addition, they bridge the porescale and the continuum scale, and their extensions can be used in multiscale modeling frameworks that are emerging. More broadly, they can be used to explore adsorption with new types of adsorbates and adsorbents. We also provide analysis of these nonstandard models.

Transport with Adsorption

The fundamental process in ECBM is the transport of multiple gas components in the coal cleats, accompanied by diffusion and adsorption into the coal matrix. Adsorption is a well known process during which the (adsorbent) gas particles adhere to a surface (of adsorbate). Adsorption is present in many natural systems and is widely used in biotechnology, pharmaceutical and chemical

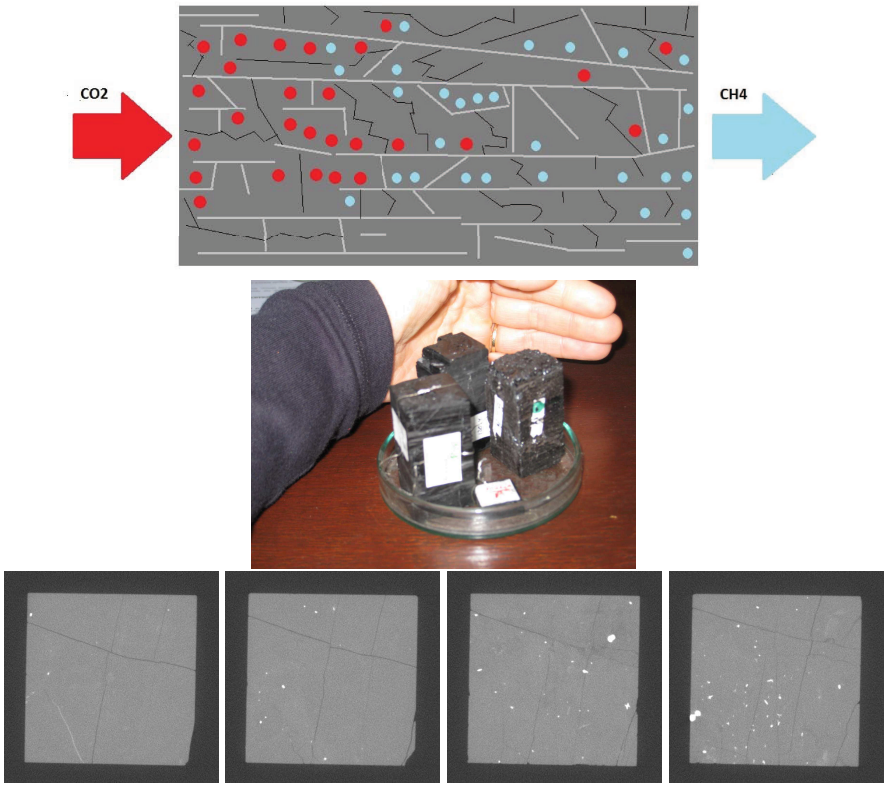

Figure 1. Top: a cartoon of coal cleat structure. Middle: coal sample held by one of the authors (MP). Bottom: porescale image of coal sample at the resolution: $30\mu\mathrm{m}$. The greyscale image shown is of two crosssections of coal, each of resolution 967×953, layers 200, 300, 400, and 500. White spots indicate mineral content. Coal sample courtesy of Ceglarska–Stefańska and Katarzyna Czerw [83, 16]; the imaging courtesy of A. Trykozko and M. Dohnalik.

engineering industry. The mathematical models of adsorption relate the amount adsorbed $a(x,t)$ to the amount $u(x,t)$ present in the fluid which transports the adsorbent. Here x denotes the position, and t denotes the time. The equilibrium models $a = a(u)$ called *isotherms* relate the bulk amounts $u(\cdot)$ to $a(\cdot)$, but do not include any considerations of local variations at pore-scale of the surface of

the adsorbate or amounts adsorbed. A well known Langmuir adsorption model

$$a(u) = V_L \frac{bu}{1+bu}$$

uses the parameters b, V_L found by fitting experimental data. (We will also use $B_L \equiv b$ to be consistent with literature.) Other nonlinear parametric algebraic relationships are formulated for various adsorbents and adsorbates.

In this paper we consider complex statistical mechanics algorithms originally proposed in [30] and followed by refined approaches in [78]; see detailed literature survey. These take into account the surface energy and the bonding energy of the particles; we reformulate them to deliver relationships $a(u)$ from statistically averaged ensembles calculated for a particular porescale geometry, or their multiple realizations.

Our focus is on the equilibrium adsorption processes coupled to the transport, thus on the hyperbolic part of the overall process. The non-equilibrium models will not be considered here; see [51, 41] for our treatement of memory terms associated with the (subscale) diffusion and the multiscale nature of porosity of coal. When the diffusion is ignored, $a(u)$ is known, and the transport velocity of gas is fixed, the nondimensional transport adsorption model is

$$u_t + a_t + u_x = 0,\ a = a(u). \tag{1}$$

Its analysis and numerical approximation follow the well-established theory for a scalar conservation law

$$w_t + f(w)_x = 0 \tag{2}$$

via a change of variables; we review these in Section 3. However, previous mathematical and numerical analysis of the advection transport with adsorption has been confined only to the adsorption isotherms in the form of simple algebraic expressions. In this paper we provide analyses of the hybrid models.

Multiple Components

When adsorption involves multiple components, then $u = (u_1, u_2, \ldots u_I)$ and $a = (a_1, a_2, \ldots a_I)$ are vectors, where I is the number of components such as methane CH4, carbon dioxide CO2, and/or nitrogen N. To obtain $a_j(u)$, it is common to extend the single-component algebraic relationships based on various assumptions and further parameter fitting. Some of the explicit algebraic

relationships $a_j(u)$ are not thermodynamically consistent and, in particular, do not satisfy Gibbs adsorption equation [18]. The thermodynamically consistent approaches can be formulated but are not given by explicit algebraic relationships.

The mathematical and computational treatment of the transport system for $I > 1$ with multicomponent adsorption is challenging due to its coupled nonlinear hyperbolic system structure. Analysis is further complicated if $a(\cdot)$ are not given by explicit algebraic relationships.

In this paper we discuss two thermodynamically consistent approaches. First we recall the Ideal Adsorbate Solution (IAS) theory, which allows to combine any single-component isotherms to deliver correct $a_j(u)$. Next we consider the pore-scale statistical mechanics-based models for single-component isotherms following [78]. We combine next the single-component adsorption isotherms produced by statistical mechanics within IAS approach. The *hybrid adsorption models* which result from this do not have a closed algebraic form, and we develop new analyses and numerical simulation results for these.

The outline of the paper is as follows. In Section 2, we first develop the overall background for multi-component adsorption and flow processes; here we pay attention to the physical principles underlying the adsorption in subsurface accompanying the flow in subsurface, and we review the different assumptions, models, and the units used in the literature. Second, in Section 3 we review the mathematical theory for the single-component adsorption models assuming equilibrium and non-equilibrium; we also define the basic computational models for single-component adsorption, and recall the principles of their analysis. Next we move to multi-component adsorption. As a first application of the theory we discuss the IAS model and provide examples. In Section 4 we introduce the porescale models based on statistical mechanics and provide their analyses. We close in Section 5.

2. Processes and Continuum Models

The majority of transport in coalbeds occurs in the cleats, accompanying the flow of gas and possibly of water, while the majority of storage occurs in the matrix where gases undergo diffusion and adsorption, close to supercritical conditions. For ECBM, the distribution of phases and components is shown in Figure 2; the components are $C = M, D, N, (W)$ methane, carbon dioxide, nitrogen, and (for wet gas models) water. The phases in which these components

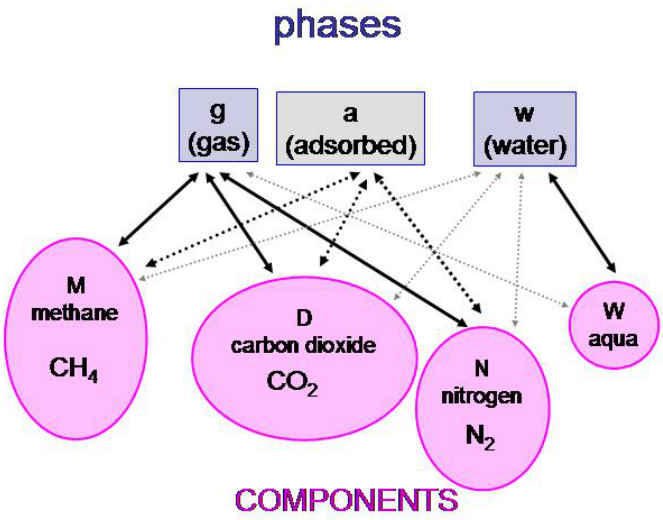

Figure 2. Phase-component distribution in ECBM.

can remain are $p = g, a, l$: gas, adsorbed gas, and liquid phase (for wet gas).

In this paper we will ignore the presence of water and consider a dry-gas model, with two components M, D, and phases g, a. Here g is the flowing (mobile) phase, and a is the adsorbed phase. Below we develop the model, paying attention to the units and different notation used in the literature. We refer to the literature listed in Table 1 for more general models.

When gases such as carbon dioxide are injected into coal seams, they make their way through the cleats into the micropore structure of the coal matrix; see Figure 1. Here they preferentially adsorb, displacing methane from adsorption sites; subsequently, this methane is transported through cleats and is available for extraction. The predominant transport mechanism in cleats (macropores) is that of advection while the transport into and out of the coal matrix occurs through diffusion into mesopores and micropores, where the gases undergo adsorption and desorption at the surface of the grains. The micropore and mesopore diffusion have been included in the classical bidisperse model [59, 31] extended to include adsorption in micropores in [13] and to realistic gas trans-

Table 1. Adsorption models relevant for ECBM. The symbol − means that the model did not have all the details. EL is the Extended Langmuir.

Model	Transport	Phases	Components	Adsorption	Isotherms	Hysteresis
[31]	compress.	2	1	Eq. & Kinetic	EL	
[28]		1	2	Eq.	EL	Yes
[68]		2	2	Kinetic	EL	
[69]	compress.	1	2	Kinetic & Multi	EL	
[82]	-	-	2	-	EL,IAS	

port models [69], with ECBM-related experimental work on the rates of kinetics in [8]. See also [31, 59, 68, 13]. The models accounting for multiscale structure of coal are, in essence, non-equilibrium models, and many are similar to the double-porosity models [3, 26] which were developed for slightly compressible flow in oil- and gas reservoirs with fractures and fissures. When advection is the predomimant transport mechanism, practical implementation results were reported for ECBM in [68, 82]. In [51, 52] we provided analysis and numerical analysis most closely related to the challenges of ECBM system, and in [42] we showed simulation results for multicomponent systems with memory. In this paper our focus is on the hyperbolic part of ECBM models and we will not include the memory terms in our models.

2.1. Comprehensive Model for Multiple Components

First we provide definitions of variables, and account carefully for different conventions from literature. Next we state the mass conservation equations, and discuss the isotherms $a(\cdot)$.

Below we only consider gas phase as the only mobile phase, thus we will simplify and drop the subscript g whenever it does not lead to a confusion.

Definitions of Variables

For multiple components and every phase $\alpha = g, a$ we have that

$$\sum_i \chi_{\alpha i} = 1, \tag{3}$$

where $\chi_{\alpha i}$ are nonnegative nondimensional variables called mass fractions of component i in phase α. We will denote $\chi_i := \chi_{gi}$. For the phase density

$\rho = \rho_g$ we write

$$\rho = \sum_i \rho_i = \sum_i \chi_i \rho, \quad \rho_i = \chi_i \rho,$$

where ρ_i are the component densities (mass per volume of mixture) with units of density [kg/m3]. The phase (and component) densities depend on the temperature, pressure, and composition of the fluid via an Equation of State (EOS) to be discussed later.

One also uses the notion of the molar mas of a component M_i ([kg/mol]). In a mixture we have its molar mass $M = \sum_i y_i M_i$ where y_i are the mole fractions defined as $y_i = \frac{M_i}{M}$. The relationship between χ_i and y_i is thus

$$y_i := \chi_i \frac{M}{M_i}$$

so that, with a simple algebra, we confirm that $\sum_k y_k \equiv 1$. Further, molar volume is related to molar mass and to the density by $V = \frac{M}{\rho}$ and for a mixture $V = \frac{\sum_i \chi_i M_i}{\rho}$. We also define frequently used molar concentrations ([mol/m3])

$$C_i := \frac{\rho_i}{M_i} \tag{4}$$

Note that C_i inherits the qualitative behavior of the density ρ_i from EOS developed below.

Equation of State

For gases, typically

$$\rho_g := \frac{M_g P_g}{RTZ(P_g, T)} := \rho_{g,o} \frac{P_g}{Z(P_g, T)} \tag{5}$$

where Z is the "compressibility factor" which depends on the pressure P_g and temperature T. The Z-factor is mildly decreasing and then increasing with pressure for pressure between 0 bar and 100 bar=6MPa. Here $\rho_0 = \frac{M_g}{RT}$ is computed using the molecular mass of the gas M_g, temperature T, and universal gas constant R. Recall that for ideal gas $Z = 1$. Furthermore, in the range of around $T \approx 300K$ the Z-factor for methane is not very far from 1, and can be assumed constant. (See [[31], *eqn.A-5*]).

In most ECBM models one assumes that $T \approx const$. Also, R, ρ_o are always constant. If we insert (5), and multiply by $\frac{1}{\rho_o}\frac{RT}{M_g}$, the resulting formulation is as in [[31], *eqn.4*], where an additional term due to the slippage effect was included.

It is natural to extend (5) to mixtures so that

$$\rho_i := \frac{M_i P_i}{ZRT}. \tag{6}$$

Here we must define the partial pressures P_i, and see that Z must depend on P and on the overall composition of the mixture (not only on P_i or y_i but on all $y_i, i = 1, \ldots I$).

Since we want $\rho = \sum_i \rho_i$, we must have

$$\rho = \frac{MP}{ZRT} = \frac{(\sum_i y_i M_i)P}{ZRT}. \tag{7}$$

Thus the natural identification follows

$$P_i = y_i P. \tag{8}$$

We also have

$$C_i = \frac{\rho_i}{M_i} = \frac{\chi_i \rho}{M_i} = \frac{y_i \rho}{M} \tag{9}$$

$$C_i = \frac{M_i P_i}{M_i ZRT} = \frac{P_i}{ZRT} = \frac{y_i P}{ZRT}. \tag{10}$$

Note that due to (3), the variables χ_i (or equivalently C_i or y_i) are not independent.

Mass Conservation Equations

The point of departure for transport models is the system

$$\frac{\partial}{\partial t}(\phi \rho_i) + \nabla \cdot (\rho_i v_g) + (1-\phi) q_{ai} = q_i, \tag{11}$$

to be solved for ρ_i or χ_i. Here q_{ai} is the rate of adsorption of component i, and v_g is the gas velocity.

Equivalently, when each (11) is divided by the constant M_i, we have

$$\frac{\partial}{\partial t}(\phi S_g C_i) + \nabla \cdot (C_i v_g) + (1-\phi)\tilde{q}_{a,i} = \tilde{q}_i,$$

which needs to be solved for C_i. Alternatively, upon multiplying by RT,w ith $Z \approx 1$, and with (8), we get

$$\frac{\partial}{\partial t}(\phi P_i) + \nabla \cdot (P_i v_g) + (1-\phi)\bar{q}_{a,i} = RT\tilde{q}_i.$$

In these formulations the adsorption isotherm $q_{a.i}$ was rescaled to $\tilde{q}_{a,i}, \bar{q}_{a,i}$, respectively. See [[28], *eqn.(2)*] and [[68], *eqn (1a)*] for equivalent formulations.

Gas velocity

In general, gas velocity in porous medium varies with pressure and the gravitational potential according to the Darcy's law

$$v_g := -\frac{k}{\mu}(\nabla P_g - \rho_g G \nabla D) \tag{12}$$

Here k is the medium permeability, μ gas viscosity, which may depend on the pressure and composition. With (12) and full EOS, the gas flow problem becomes a degenerate nonlinear parabolic system to be solved for P_g; we will not address this here. Instead, in what follows we assume

$$v_g \approx const, \tag{13}$$

i.e., that the flow is steady, and the pressure distribution $P_g(x,t) = P_g(x)$ is also steady and known. This is as in [28] where it seems (see Section 4.1) that in a numerical model the authors solve for P_g and v_g, albeit infrequently, compared to the time steps for adsorption. Solving for pressure means solving an equation obtained from summing all the I mass conservation equations, plus $I-1$ adsorption equations.

Adsorption Relationships

To complete the model we need to determine $q_{a,i}$ or its rescaled variants depending on χ_i, y_i, or p_i. The equilibrium adsorption assumption, postulates

$$q_{a.i} := \frac{\partial}{\partial t} a_i(P_1, \ldots P_I), \tag{14}$$

and that the gas amounts in the mobile phase and those adsorbed on the surface of adsorbent are in fixed proportion given by $a_i(P_1, \ldots P_I)$.

2.1.1.

With the assumption (13) we analyze and approximate the ECBM system (11) with (14) as a nonlinear hyperbolic system.

2.2. Sorption Isotherms

Now we discuss the mass rate of adsorption q_{ai} or the appropriately scaled quantities $\bar{q}_a$, $\tilde{q}_a$. We ignore any such scaling below, since it can be absorbed in the leading constants.

2.2.1. Single Component Isotherms

The widely used Langmuir monolayer isotherm is

$$a(P_g) = V_L \frac{bP_g}{1 + bP_g} = V_L \frac{P_g}{P_L + P_g}. \tag{15}$$

The coefficients V_L are the Langmuir volume capacity and b Langmuir constant; see, e.g., [[68], *eqn.(4)*]. Equivalently, P_L is so called Langmuir pressure, and we have $b = \frac{1}{P_L}$; see [[31], *eqn.(12)*]. The constants V_L, b are found experimentally from the data of amount (volume) adsorbed $a(P_g)$ as a function of P_g. This is enabled simply by a linear regression fit of $\frac{P_g}{a(P_g)}$ to $\frac{1}{V_L}(P_g + P_L)$. In addition, V_L provides the horizontal asymptote (maximum capacity) for the isotherm, and $bV_L = \frac{V_L}{P_L}$ provides the slope of the isotherm at 0. V_L is typically given in units of adsorbed amount per mass of adsorbent. In Table 2 we provide V_L, b data for the Langmuir isotherms for CH4 and CO2.

Other isotherms such as Henry's, Freundlich, or BET are well known [18]. Since data for ECBM has mostly been fit to (15), we do not review these here.

2.2.2. Multiple Component Isotherms

For multiple components, various extensions are proposed. For example, the authors in [28] propose an extension of the Langmuir single-component isotherm (15) and define

$$a_i(P_1, \ldots P_I) := V_{L,i} \frac{b_i P_i}{1 + \sum_k b_k P_k}. \tag{16}$$

The extended Langmuir model (EL) (16) is a very simple algebraic model. It only requires the parameters $b_i, V_{L,i}$, which are fit to experimental data.

Table 2. Parameters of single-component isotherms from literature. (a) Jincheng coal. (b) Luan coal.

Source	V_L	$b = B_L$ **or** $1/b = P_L$	
[31]	CH4	V_L=[18.6,34.3] scf/cu ft	$1/b = P_L$=167.5 psia
[28]	CH4	V_L=811 SCF/ton	b=0.000237 1/psia
	CO2	V_L=1760 SCF/ton	b=0.000521 1/psia
[68]	CH4	V_L=25.57 cu m/cu m	P_L=2.07 MPa
	CO2	V_L=47.73 cu m/ cum	P_L=1.38 MPa
[67]	CH4	V_L=0.80 mol/l	b = 0.23 1/MPa
	CO2	V_L=1.60 mol/l	b= 0.464 1/1MPa
[6]	CH4	$V_L \in$[0.5,1] mmol/g-coal	$P_L \in$[690,3450] kPa
	CO2	[0.5,2.5] mmol/g-coal	[3450,6900] kPa
[82]$^{(a)}$	CH4	V_L = 1.183 mmol/g	P_L = 0.69 MPa
	CO2	V_L=1.392 mmol/g	P_L=0.33 MPa
[82]$^{(b)}$	CH4	V_L=1.017 mmol/g	P_L = 0.70 MPa
	CO2	V_L=0.949 mmol/g	P_L = 0.23 MPa

However, EL appears thermodynamically inconsistent unless $V_{L,i}$ are equal to each other for each i [18], because Gibbs isotherm equation is not satisfied. The extended Langmuir model is formulated ad-hoc from single-component isotherms based on the assumption of equality of adsorption and desorption rates, but it does not account for any interaction of the molecules of the adsorbate with each other and with the molecules of bulk phase.

Other choices are available. In particular, various authors in ECBM literature [6, 13, 82] use the IAS (Ideal Adsorbate Solution) theory which follows directly from Gibbs isotherm equation and is also known as Myers-Prausnitz theory.

2.2.3. IAS Model for Multicomponent Adsorption

The IAS model for multicomponent adsorption can be formulated for any number I of components and for any collection of single-component isotherms, possibly different for each component. Here we follow [18].

The IAS model assumes only the knowledge of single-component isotherms

$$a_i^0(P_i) \equiv a_i(0, \ldots, 0, P_i, 0, \ldots 0). \tag{17}$$

where a_i^0 denotes the amount of i adsorbed in the absence of other components. IAS derives a system of algebraic equations from the principle of equality of chemical potentials in the bulk phase and in the adsorbed phase which is stated in Gibbs adsorption isotherm equation. The derivation of IAS follows principles similar to the vapor-liquid equilibria represented by Raoult's law. As a result of IAS, the values of $a_i(\cdot)$ are defined implicitly rather than explicitly.

We first define

$$z := \int_0^{P_i^0} \frac{a_i^0(p)}{p} dp. \tag{18}$$

Next, we find the relationship $P_i^0(z)$ by inverting $z(P_i^0)$. The analytical form for $P_i^0(z)$ is only available for special cases of a_i^0 such as Langmuir isotherm. In that case, we have $P_i^0(z) = \frac{1}{b_i}\left[exp(\frac{z}{V_{L,i}}) - 1\right]$. In general, $z(P_i^0)$ or its inverse have to be found by numerical integration.

Next, assume we are given $P_1, P_2, \ldots P_I$ as independent variables. To find $z(P_1, P_2, \ldots, P_I)$ we solve

$$F(z) = \sum_i \frac{P_i}{P_i^0(z)} - 1 = 0 \tag{19}$$

In general, this is done by a nonlinear numerical solver. The Jacobian for the Newton-Raphson iteration of (19) requires, in particular, that we compute the Jacobian

$$F'(z) = -\sum_i P_i \frac{(P_i^0(z))'}{(P_i^0(z))^2}.$$

Once we know z, we have a definition

$$a_i(P_1, \ldots P_I) := P_i \frac{\partial z}{\partial P_i}. \tag{20}$$

This calculation requires $\frac{\partial z}{\partial P_i}$. We find $\frac{\partial z}{\partial P_i} = -\frac{1}{P_i^0}/F'(z)$, which follows from implicit differentiation of (19) with respect to P_i

$$\frac{1}{P_i^0} + \left[-\sum_i P_k \frac{(P_k^0(z))'}{((P_k^o(z)))^2}\right] \frac{\partial z}{\partial P_k} = 0.$$

2.3. Model Summary and Illustration

The multicomponent transport model from Section 2.1.1, upon scaling and nondimensionalization, in one spatial dimension, is

$$\frac{\partial}{\partial t}(P_i + a_i(P_1, P_2, \dots P_I)) + \frac{\partial P_i}{\partial x} = 0, \tag{21a}$$

The system needs initial conditions for each component

$$P_i(x, 0) = P_{i,init}(x), \tag{21b}$$

and requires a definition of the isotherms

$$a_i = a_i(P_1, P_2, \dots P_I). \tag{21c}$$

We do not explicitly address boundary conditions even though the spatial region $x \in \Omega \in R^d$ in which transport takes place is, in all practical cases, bounded. To avoid handling boundary conditions we assume that the initial data $P_{i,init}$ has compact support in $\mathbb{R}^d$, and in simulations we adjust the "observation window" accordingly.

The model (21) and its numerical approximation will be analyzed in Section 3. In particular, we consider there the IAS isotherms a_i. In Section 4 we consider and analyze a hybrid model for a_i based on statistical mechanics.

2.3.1. Simulation with EL

We provide now an illustration. We consider the dynamics similar to that encountered in ECBM reported in [28], but with $I = 2$, and CH4 denoted by $i = 1$ and CO2 denoted by $i = 2$. The isotherms a_1, a_2 are chosen as extended Langmuir (16) with the coefficients which mimick those for CH4 and CO2 from Table 2. We also set

$$\begin{aligned} P_{1,init}(x) &= H(x) = \begin{cases} 1, & x \geq 0 \\ 0, & x < 0 \end{cases} \\ P_{2,init}(x) &= 1 - H(x), \end{aligned}$$

where we used the Heaviside function $H(x)$. This case illustrates the displacement of methane CH4 by carbon dioxide CO2 in a reservoir initially filled with CH4. The simulation proceeds for $x \in [0, 1], t \in (0, T]$, with $T = 0.6$. The discretization parameters are $\Delta x = 0.01, \Delta t \approx 0.05$.

In Sections 3 and 4 we consider and analyze the isotherms provided by IAS and hybrid models.

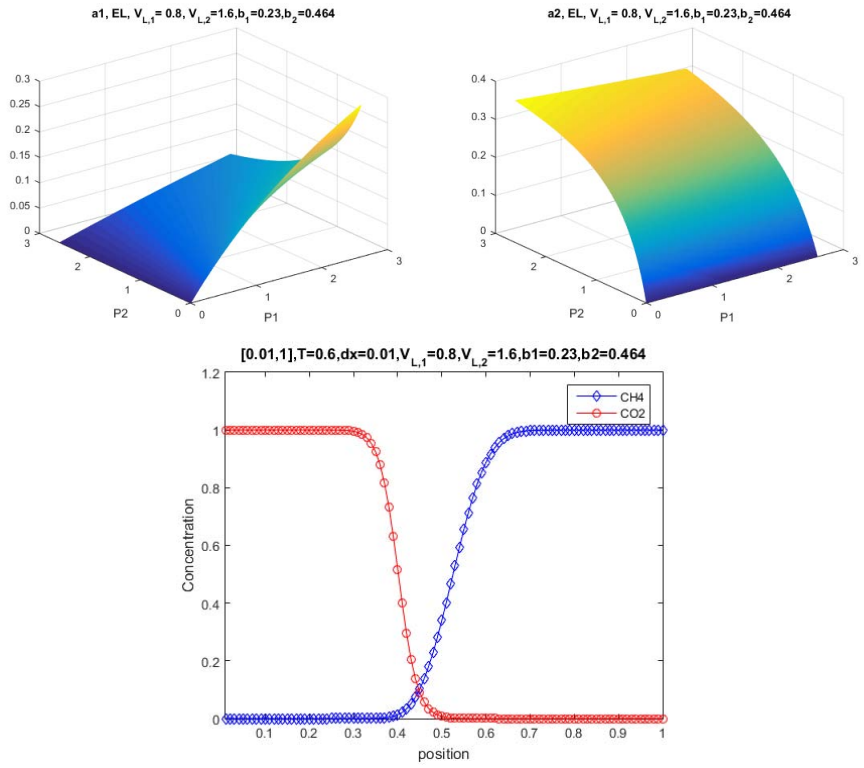

Figure 3. Isotherms and the corresponding transport solution for Extended Langmuir model (16). The parameters of the isotherms and of the simulation are as in Section 2.3.1. In particular, we use $V_{L,1} = 0.8, b_1 = 0.23, b_2 = 0.464, V_{L,2} = 1.6$, and these are similar to those used for CH4 and CO2, respectively.

3. Analysis of Transport with Adsorption and IAS

In this section we provide mathematical details concerning the multicomponent adsorption system (21) for the case $I = 2$ and one spatial variable.

We start by recalling well known theory of scalar conservation laws and hyperbolic systems which we apply to a transformed version of (21) and discuss the conditions upon which it is hyperbolic. Next we provide an explicit estimate of the eigenvalues which are helpful in establishing the stability of the numerical

schemes.

Next we specialize and consider the IAS system to which we apply the theory. The difficulty here is that the IAS multicomponent isotherms are defined implicitly, thus additional analysis has to be provided.

3.1. Analysis and Numerical Models for Conservation Laws

We consider first the well-known mathematical framework for the conservation law in $d = 1$

$$w_t + f(w)_x = 0, \quad w(x,0) = w_0(x) \tag{22}$$

with an increasing and convex flux function $f(\cdot)$. It is well known [34] that its solutions develop singularities in finite time from smooth initial data. In particular, a solution with $w_0(x) = exp(-x^2)$ develops a forward facing discontinuity (shock) with a backward facing smooth wave (rarefaction). For this reason, one defines the weak solutions to (22) to include the physically meaningful singular, i.e., non-classical solutions. Out of these, only the entropy solutions are defined to exclude, e.g., unphysical backward facing shocks. We refer to [21] or to [35] for comprehensive treatment of conservation laws and systems.

A discontinuity in (22) travels with the speed σ determined from the Rankine-Hugoniot condition

$$\sigma = \frac{[f]}{[w]} = \frac{f(w_R) - f(w_L)}{w_R - w_L}, \tag{23}$$

where $[f], [w]$ denote the jump fo the flux function and of the primary unknown across the discontinuity, respectively, and w_L, w_R are the left and right states.

An appropriate numerical method for (22) needs to be conservative and stable. The numerical discretization, via the popular first order Godunov method is

$$w_j^n = w_j^{n-1} - \lambda \left[f(w_j^{n-1}) - f(w_{j-1}^{n-1}) \right], \tag{24}$$

where $\lambda = \frac{\Delta t}{\Delta x}$, Δt is the time step, and Δx is the spatial discretization parameter. The discretization is defined at the discrete spatial and temporal points $x_j = j\Delta x, t_n = n\Delta t$ and delivers approximations $w_j^n \approx w(x_j, t^n)$. The scheme starts with the values $w_j^0 = w_{init}(x_j)$. This Godunov scheme is stable provided that for any w,

$$0 \leq \lambda f'(w) \leq 1. \tag{25}$$

For a general nonlinear flux function and a smooth enough solution, the Godunov method is (at most) first order accurate.

Let $\vec{\mathbf{f}} : \mathbb{R}^p \to \mathbb{R}^p$, $x \in \mathbb{R}$, $t > 0$. If the solutions are smooth enough, the system

$$\mathbf{w}_t + \vec{\mathbf{f}}(\mathbf{w})_x = 0 \tag{26}$$

can be written as

$$\mathbf{w}_t + \mathbf{A}(\mathbf{w})\mathbf{w}_x = 0, \tag{27}$$

where $A(\mathbf{w}) = D\vec{\mathbf{f}}(\mathbf{w})$. We denote by $(\lambda_k(\mathbf{w}))_{k=1}^p$ the eigenvalues for $A(\mathbf{w})$.

Definition 3.1. *The system* (26) *is* strictly hyperbolic *if for any* $\mathbf{w} \in \mathbf{\Omega}$, *the Jacobian matrix*

$$\mathbf{A}(\mathbf{w}) = \left(\frac{\partial \mathbf{f_i}}{\partial \mathbf{w_j}}(\mathbf{w})\right)_{\mathbf{1 \le i,j \le p}}$$

has p *distinct eigenvalues* $\lambda_1(\mathbf{w}) < \lambda_{\mathbf{2}}(\mathbf{w}) < \cdots < \lambda_{\mathbf{p}}(\mathbf{w})$.

In general, the solution profiles for (26) are complicated, especially if the eigenvalues of the Jacobian have different signs. A numerical solver such as Godunov method must use a local Riemann solver to resolve the wave interactions at every cell resulting from the left and right states. However, if the eigenvalues of the Jacobian have the same sign, one can consider a straightforward extension of the scalar Godunov scheme (24) to the multicomponent case.

3.2. Analysis and Numerics for Transport with Adsorption, $I = 1$

From now on we assume that the unknowns in our model are the (partial) pressures P_i. The scalar version of the model (21) is

$$\frac{\partial}{\partial t}(P + a(P)) + P_x = 0. \tag{28}$$

If the solutions are smooth, via a change of variable $w = P + a(P)$, and setting $f'(w) = \dfrac{1}{1 + a'(P)}$ and requiring $f(0) = 0$, we obtain (22).

It is easy to show that if $a(\cdot)$ is increasing concave, then $f(\cdot)$ is increasing convex, and the character of solutions is similar to that discussed in Section 3.1.

In particular, for the Langmuir model we quickly check that $a(\cdot)$ given by (15) is smooth, strictly increasing, concave, and Lipschitz, via

$$a'(P) = \frac{bV_L}{(1+bP)^2},$$

and $0 < a'(P) \le bV_L$. Also, $0 < f'(w) = \dfrac{1}{1+a'(P)} \le 1$.

For discontinuous solutions we consider weak solutions, and determine directly the speed σ of propagation of discontinuity deriving

$$\sigma = \frac{[P]}{[P+a(P)]} = \frac{[f]}{[w]}, \tag{29}$$

which is formally consistent with the usual Rankine-Hugoniot condition (23). See [42] for details.

3.2.1. Numerical Scheme for Transport with Adsorption

In spite of formal equivalence of (28) to (22), it is better solve it in the original form (28). For this, we propose the scheme

$$P_j^{n+1} + a(P_j^{n+1}) = P_j^n + a(P_j^n) - \lambda \left(P_j^n - P_{j-1}^n\right). \tag{30}$$

In the scheme we actually calculate explicitly the left hand side

$$W_j^{n+1} = P_j^{n+1} + a(P_j^{n+1}), \tag{31}$$

and this is done for every j. Since our primary unknown is P_j^{n+1}, we must solve (31), given W_j^{n+1} for P_j^{n+1}. For some isotherms $a(\cdot)$ this can be done algebraically, and for the general case we implement a local Newton solver. Usually only a few iterations suffice, since $I + a(\cdot)$ is a smooth bijective function. A good initial guess for this local solver is provided by the zero of a linear model of $a(\cdot)$ at 0.

Based on the discussion above and $0 < f' \le 1$, we see that the stability restriction for the numerical schemes is simply $\lambda \le 1$ or

$$\Delta t \le \Delta x(1 + a'(P_j^n)) \text{ for all } P_j^n. \tag{32}$$

3.3. Analysis for Multicomponent Transport with Adsorption, $I = 2$

Now we consider (21) with $I = 2$. We get to the form (26) by the change of variables $w_i = P_i + a_i(\mathbf{P})$, for $i = 1, 2$. where $\mathbf{P} = (P_1, P_2)$. We define $\mathbf{w} = (w_1, w_2)$, $\vec{a}(\mathbf{P}) := \begin{pmatrix} a_1(\mathbf{P}) \\ a_2(\mathbf{P}) \end{pmatrix}$ and $\mathbf{P} = \vec{\mathbf{f}}(\mathbf{w})$, where $\vec{\mathbf{f}}(\mathbf{w}) = (I + \vec{a})^{-1}\mathbf{w} = \mathbf{P}$. Notice that $I + \vec{a} : \mathbb{R}^2 \to \mathbb{R}^2$ is nonlinear and its components are continuously differentiable in the domain of interest.

With this change of variables, the adsorption (21) is in the form (26). The change of variables is formally only valid, as we nentioned in Section 3.1, if the solutions are smooth enough; see also the discussion of shock speed calculation in (29). To check if the system is hyperbolic, we inspect the Jacobian

$$\mathbf{A}(\mathbf{w}) = \mathbf{B}^{-1}(\mathbf{w}), \tag{33}$$

where $\mathbf{B}$ is given by, with $B_{ij} = \frac{\partial a_i}{\partial P_j}$, as

$$\mathbf{B}(\mathbf{P}) = \begin{pmatrix} 1 + B_{11} & B_{12} \\ B_{21} & 1 + B_{22} \end{pmatrix}.$$

Lemma 3.1. *The system* (27) *is strictly hyperbolic if*

$$B_{12}B_{21} = \left(\frac{\partial a_1}{\partial P_2}\right)\left(\frac{\partial a_2}{\partial P_1}\right) > 0 \tag{34}$$

In addition, if

$$d^* = B_{11}B_{22} - B_{12}B_{21} \geq 0. \tag{35}$$

holds, then

$$\lambda_-(\mathbf{B}; \mathbf{P}) \geq 1. \tag{36}$$

Proof. The characteristic polynomial for $\mathbf{B}$ is given by

$$\lambda^2 - \lambda(2 + B_{11} + B_{22}) + (1 + B_{11})(1 + B_{22}) - B_{12}B_{21}.$$

and its eigenvalues are

$$\begin{aligned} \lambda_\pm(\mathbf{B}; \mathbf{P}) &= \frac{1}{2}\left[2 + B_{11} + B_{22} \pm \sqrt{(B_{11} - B_{22})^2 + 4B_{12}B_{21}}\right] \\ &= 1 + \frac{B_{11} + B_{22}}{2} \pm \sqrt{\left(\frac{B_{11} + B_{22}}{2}\right)^2 - (B_{11}B_{22} - B_{12}B_{21})}. \end{aligned} \tag{37}$$

In order for the eigenvalues to be real and distinct, and system to be hyperbolic, we need $(B_{11} - B_{22})^2 > -4B_{12}B_{21}$. This is guaranteed if $B_{12}B_{21} > 0$.

In addition, if (35) holds, we have

$$\lambda_-(\mathbf{B};\mathbf{P}) = 1 + \frac{B_{11}+B_{22}}{2} - \sqrt{\left(\frac{B_{11}+B_{22}}{2}\right)^2 - (B_{11}B_{22} - B_{12}B_{21})}, \quad (38)$$

Clearly, by (35) the second term under the square root is nonpositive, and the conclusion follows. □

For most adsorption systems the conditions (34)–(35) hold. In particular, for the Extended Langmuir system and other known algebraic expressions for isotherms, one can calculate the partial derivatives $\frac{\partial a_i}{\partial P_j}$ and check (34) and (35) directly.

For general adsorption isotherms, the conditions (34) and (35) make physical sense, since the amount adsorbed of a component should increase with its partial pressure. In turn, in competitive adsorption, the amount adsorbed of component i should decrease with the increase of partial pressure of other components, and there should be a symmetry in the signs of B_{12} and B_{21}.

However, in a particular model without an explicit algebraic expression one should verify if the desired qualitative properties hold. In what follows we will discuss the isotherms $a_i(P_1, P_2)$ derived from IAS as well as those from statistical mechanics to see if (34) and (35) hold.

3.3.1. Numerics for the Adsorption System

Knowing the eigenvalues $\lambda(\mathbf{B};\mathbf{P})$ of $\mathbf{B}$, we can calculate their algebraic inverses, i.e., the eigenvalues $\lambda(\mathbf{A};\mathbf{w})$ for $A(\mathbf{w})$. For many adsorption systems, as mentioned above, it is easy to show that these are positive.

If so, the construction of the Godunov scheme takes the simple upwind form

$$P_{1,j}^{n+1} + a_1\left(P_{1,j}^{n+1}, P_{2,j}^{n+1}\right) = P_{1,j}^{n} + a_1\left(P_{1,j}^{n}, P_{2,j}^{n}\right) - \frac{\Delta t}{\Delta x}\left(P_{1,j}^{n} - P_{1,j-1}^{n}\right), \quad (39)$$

$$P_{2,j}^{n+1} + a_2\left(P_{1,j}^{n+1}, P_{2,j}^{n+1}\right) = P_{2,j}^{n} + a_2\left(P_{1,j}^{n}, P_{2,j}^{n}\right) - \frac{\Delta t}{\Delta x}\left(P_{2,j}^{n} - P_{2,j-1}^{n}\right), \quad (40)$$

where $P_{k,j}^n \approx P_k(x_j, t_n)$ for $k = 1, 2$. As before, we have to implement a local 2×2 nonlinear solver to get both $P_{k,j}^n, k = 1, 2$ from the left hand side(s) of (39)-(40).

The stability condition for a numerical scheme for the system is [21]

$$\lambda \max_{k=\pm} \left| \frac{1}{\lambda_k(\mathbf{B}; \mathbf{P}^{\mathbf{n}}_{\mathbf{j}})} \right| \leq \frac{1}{2} \quad \text{at each } \mathbf{P}^{\mathbf{n}}_{\mathbf{j}}.$$

This gives the following condition for the time step

$$\Delta t \leq \frac{\Delta x}{2} \min_{k=\pm} \left| \lambda_k(\mathbf{B}; \mathbf{P}^{\mathbf{n}}_{\mathbf{j}}) \right| \quad \text{at each } \mathbf{P}^{\mathbf{n}}_{\mathbf{j}}. \tag{41}$$

Since the eigenvalues of a nonlinear system in general depend on the unknown solution, it is useful to know if one can derive a CFL condition which does not depend on (P_1, P_2). Such a condition is possible, e.g., if (35) holds and Lemma 3.1 applies. In addition, if (36) holds, we have

$$\frac{\Delta t}{\Delta x} \leq \frac{1}{2}. \tag{42}$$

We will confirm that this is indeed works for the IAS system and for the MFEQ system.

3.4. Analysis of the Extended Langmuir System

For the extended Lagmuir system (16) we calculate

$$\frac{\partial a_1}{\partial P_1} = \frac{b_1 V_{L,1}(1 + b_2 P_2)}{(1 + b_1 P_1 + b_2 P_2)^2}, \; \frac{\partial a_1}{\partial P_2} = \frac{-b_1 b_2 V_{L,1} P_1}{(1 + b_1 P_1 + b_2 P_2)^2},$$

and the expressions for $\dfrac{\partial a_2}{\partial P_i}, i = 1, 2$, follow analogously. From these calculations we see that Lemma 3.1 applies. Thus the extended Langmuir system is strictly hyperbolic, and the eigenvalues $\lambda_-(\mathbf{B}; \mathbf{P})$ for any $\mathbf{P}$ are bounded below by 1.

3.5. Analysis of IAS Adsorption System

We consider the transport system

$$\frac{\partial}{\partial t}(P_1 + a_1^{IAS}(\mathbf{P})) + \frac{\partial P_1}{\partial x} = 0, \tag{43}$$

$$\frac{\partial}{\partial t}(P_2 + a_2^{IAS}(\mathbf{P})) + \frac{\partial P_2}{\partial x} = 0, \tag{44}$$

with a_i^{IAS} given by the IAS algorithm from Section 2.2.3.

To check its hyperbolicity and to calculate its eigenvalues, we wish to apply Lemma 3.1. However, since the isotherms are defined implicitly, some work is required.

Proposition 3.1. *The system* (43)–(44) *is strictly hyperbolic in the region*

$$P_1 > 0, \;\; P_2 > 0. \tag{45}$$

In addition, in this region, if

$$a_1^\circ > 0, \; a_2^\circ > 0, \;\; (a_1^\circ)'(\cdot) > 0, (a_2^\circ)'(\cdot) > 0 \tag{46}$$

are nonnegative functions, then the lower bound (36) *holds.*

Proof. To apply Lemma 3.1, and prove the first part, we need either (34) or (35) to hold.

$$\left(\frac{\partial a_1^{IAS}}{\partial P_2}\right)\left(\frac{\partial a_2^{IAS}}{\partial P_1}\right) > 0.$$

We calculate easily from (20)

$$\left(\frac{\partial a_1^{IAS}}{\partial P_2}\right)\left(\frac{\partial a_2^{IAS}}{\partial P_1}\right) = P_1 P_2 \left(\frac{\partial^2 z}{\partial P_1 \partial P_2}\right)^2 > 0. \tag{47}$$

Thus the first part of the proposition holds if (45) holds.

To prove the second part, we proceed as in Lemma 3.1, but the calculations are extensive. We calculate $B_{ij} = \frac{\partial a_i^{IAS}}{\partial P_j}$. From (18) we have

$$\frac{\partial z}{\partial P_i^\circ} = \frac{a_i^\circ(P_i^\circ)}{P_i^\circ}, \text{ for } i = 1, 2.$$

Now from (19) for $I = 2$ and $z = z(P_1, P_2)$, by implicit differentiation we get

$$\frac{\partial z}{\partial P_1} = \frac{a_1^\circ a_2^\circ P_2^\circ}{D}, \;\; \frac{\partial z}{\partial P_2} = \frac{a_1^\circ a_2^\circ P_1^\circ}{D}. \tag{48}$$

where $D = a_1^\circ P_2 P_1^\circ + a_2^\circ P_1 P_2^\circ$. (Here and below we apply a slight abuse of notation and drop the unknowns in $a_i^\circ = a_i^\circ(P_i^\circ)$.) Thus $\dfrac{\partial z}{\partial P_i} \geq 0$ for $i = 1, 2$. Further, from (20) we calculate

$$\frac{\partial a_1^{IAS}}{\partial P_1} = \frac{\partial z}{\partial P_1} + P_1 \frac{\partial^2 z}{\partial P_1^2}, \quad \frac{\partial a_1^{IAS}}{\partial P_2} = P_1 \frac{\partial^2 z}{\partial P_2 \partial P_1}. \tag{49}$$

with the other derivatives given analogously. Next we need the derivatives $\frac{\partial^2 z}{\partial P_i}$ and $\frac{\partial^2 z}{\partial P_i \partial P_j}$ in terms of $a_1^\circ,\ a_2^\circ,\ P_1^\circ,\ P_2^\circ,\ P_1$ and P_2. To compute $\frac{\partial^2 z}{\partial P_1^2}$, by (48) we have

$$D\frac{\partial z}{\partial P_1} = a_1^\circ a_2^\circ P_2^\circ.$$

Differentiating both sides we get

$$D\frac{\partial^2 z}{\partial P_1^2} = \frac{\partial (a_1^\circ a_2^\circ P_2^\circ)}{\partial P_1} - \frac{\partial D}{\partial P_1}\frac{\partial z}{\partial P_1}. \tag{50}$$

On the other hand, we have

$$\frac{\partial (a_1^\circ a_2^\circ P_2^\circ)}{\partial P_1} = \frac{\partial z}{\partial P_1}\left[\frac{da_1^\circ}{dP_1^\circ}\frac{P_1^\circ}{a_1^\circ}a_2^\circ + \frac{da_2^\circ}{dP_2^\circ}\frac{P_2^\circ}{a_2^\circ}a_1^\circ + a_1^\circ\right]P_2^\circ, \tag{51}$$

Also,

$$\frac{\partial D}{\partial P_1} = P_1^\circ P_2 \frac{\partial z}{\partial P_1}\left(\frac{da_1^\circ}{dP_1^\circ}\frac{P_1^\circ}{a_1^\circ} + 1\right) + P_2^\circ P_1 \frac{\partial z}{\partial P_1}\left(\frac{da_2^\circ}{dP_1^\circ}\frac{P_2^\circ}{a_2^\circ} + 1\right) + a_2^\circ P_2^\circ. \tag{52}$$

Finally, substituting (51) and (52) in (50) and doing some algebraic manipulations we obtain

$$\frac{\partial^2 z}{\partial P_1^2} = \frac{1}{D^3}\left[SP_1^\circ (P_2^\circ)^3 + (a_1^\circ)^3 a_2^\circ P_1^\circ (P_2^\circ)^2 P_2 - 2(a_1^\circ)^2 (a_2^\circ)^2 P_1^\circ (P_2^\circ)^2 P_2 - a_1^\circ (a_2^\circ)^3 (P_2^\circ)^3 P_1\right], \tag{53}$$

where

$$S = \frac{da_1^\circ}{dP_1^\circ}(a_2^\circ)^3 P_1 + \frac{da_2^\circ}{dP_2^\circ}(a_1^\circ)^3 P_2.$$

To compute $\frac{\partial^2 z}{\partial P_2 \partial P_1}$, we note that

$$D\frac{\partial^2 z}{\partial P_2 \partial P_1} = \frac{\partial (a_1^\circ a_2^\circ P_2^\circ)}{\partial P_2} - \frac{\partial D}{\partial P_2}\frac{\partial z}{\partial P_1}. \tag{54}$$

$$\frac{\partial (a_1^\circ a_2^\circ P_2^\circ)}{\partial P_2} = \frac{\partial z}{\partial P_2}\left[\frac{da_1^\circ}{dP_1^\circ}\frac{P_1^\circ}{a_1^\circ}a_2^\circ + \frac{da_2^\circ}{dP_2^\circ}\frac{P_2^\circ}{a_2^\circ}a_1^\circ + a_1^\circ\right]P_2^\circ, \tag{55}$$

and

$$\frac{\partial D}{\partial P_2} = P_1^\circ P_2 \frac{\partial z}{\partial P_2}\left(\frac{da_1^\circ}{\partial P_1^\circ}\frac{P_1^\circ}{a_1^\circ}+1\right) + P_2^\circ P_1 \frac{\partial z}{\partial P_2}\left(\frac{da_2^\circ}{dP_2^\circ}\frac{P_2^\circ}{a_2^\circ}+1\right) + a_1^\circ P_2^\circ. \quad (56)$$

Substituting (55) and (56) in (54) we get

$$\frac{\partial^2 z}{\partial P_2 \partial P_1} = \frac{(P_1^\circ)^2 (P_2^\circ)^2}{D^3}\Big(S - (a_1^\circ)^2 (a_2^\circ)^2\Big)^2. \quad (57)$$

Putting it all together have the following expressions for $\frac{\partial a_i^{IAS}}{\partial P_i}$:

$$\begin{aligned}
\frac{\partial a_1^{IAS}}{\partial P_1} &= \frac{P_1^\circ P_2^\circ}{D^3}(S(P_2^\circ)^2 P_1 + (a_1^\circ)^3 a_2^\circ P_1^\circ P_2^\circ P_2),\\
\frac{\partial a_2^{IAS}}{\partial P_2} &= \frac{P_1^\circ P_2^\circ}{D^3}(S(P_1^\circ)^2 P_2 + (a_2^\circ)^3 a_1^\circ P_1^\circ P_2^\circ P_1),\\
\frac{\partial a_1^{IAS}}{\partial P_2} &= \frac{P_1 (P_1^\circ)^2 (P_2^\circ)^2}{D^3}(S - (a_1^\circ)^2 (a_2^\circ)^2),\\
\frac{\partial a_2^{IAS}}{\partial P_1} &= \frac{P_2 (P_1^\circ)^2 (P_2^\circ)^2}{D^3}(S - (a_1^\circ)^2 (a_2^\circ)^2).
\end{aligned}$$

Setting $d = (B_{11} - B_{22})^2 + 4B_{12}B_{21}$ we rewrite

$$\begin{aligned}
d &= B_{11}^2 - 2B_{11}B_{22} + B_{22}^2 + 4B_{12}B_{21}\\
&= B_{11}^2 - 2B_{11}B_{22} + 2B_{11}B_{22} - 2B_{11}B_{22} + B_{22}^2 + 4B_{12}B_{21}\\
&= (B_{11} + B_{22})^2 - 4d^*.
\end{aligned}$$

We can now show that (35) holds under certain assumptions. We expand

$$\begin{aligned}
d^* &= \frac{(P_1^\circ)^2 (P_2^\circ)^2}{D^6}(S(P_2^\circ)^2 P_1 + (a_1^\circ)^3 (a_2^\circ) P_1^\circ P_2^\circ P_2)(S(P_1^\circ)^2 P_2 + (a_2^\circ)^3 (a_1^\circ) P_1^\circ P_2^\circ P_1)\\
&\quad - \frac{P_1 P_2 (P_1^\circ)^4 (P_2^\circ)^4}{D^6}(S - (a_1^\circ)^2 (a_2^\circ)^2)^2\\
&= \frac{(P_1^\circ)^2 (P_2^\circ)^2}{D^6}\Big(S(P_1^\circ)^2 (P_2^\circ)^2 P_1 P_2 + S(P_2^\circ)^3 (a_2^\circ)^3 (a_1^\circ) P_1^2 + S(P_1^\circ)^3 (a_2^\circ)(a_1^\circ)^3 P_2^2\\
&\qquad + (a_1^\circ)^4 (a_2^\circ)^4 (P_1^\circ)^2 (P_2^\circ)^2 P_1 P_2 - P_1 P_2 (P_1^\circ)^2 (P_2^\circ)^2 (S - (a_1^\circ)^2 (a_2^\circ)^2)^2\Big)\\
&= \frac{(P_1^\circ)^2 (P_2^\circ)^2}{D^3}\Big(S(P_1^\circ)^2 (P_2^\circ)^2 P_1 P_2 + S(P_2^\circ)^3 (a_2^\circ)^3 (a_1^\circ) P_1^2 + S(P_1^\circ)^3 (a_2^\circ)(a_1^\circ)^3 P_2^2\\
&\qquad + (a_1^\circ)^4 (a_2^\circ)^4 (P_1^\circ)^2 (P_2^\circ)^2 P_1 P_2 - S(P_1^\circ)^2 (P_2^\circ)^2 P_1 P_2 + 2S(a_1^\circ)^2 (a_2^\circ)^2 (P_1^\circ)^2 (P_2^\circ)^2 P_1 P_2\\
&\qquad\qquad - (a_1^\circ)^4 (a_2^\circ)^4 (P_1^\circ)^2 (P_2^\circ)^2 P_1 P_2\Big)\\
&= \frac{(P_1^\circ)^2 (P_2^\circ)^2}{D^3}\Big(S(P_2^\circ)^3 (a_2^\circ)^3 (a_1^\circ) P_1^2 + S(P_1^\circ)^3 (a_2^\circ)(a_1^\circ)^3 P_2^2\\
&\qquad\qquad + 2S(a_1^\circ)^2 (a_2^\circ)^2 (P_1^\circ)^2 (P_2^\circ)^2 P_1 P_2\Big).
\end{aligned}$$

We can finally see that under the assumptions of the Proposition, the second part of its conclusion holds. □

We have therefore shown that as long as the single-component isotherms a_i^0 are positive and strictly increasing, the IAS system is strictly hyperbolic in the region $P_1 P_2 > 0$, and the eigenvalues are positive. In addition, the minimum eigenvalue is bounded below by 1, and the CFL constraint for the numerical solution has the simple form (42).

3.6. Results: Simulations of Transport with IAS Isotherms

To illustrate the results above, we set up isotherm calculations followed by the transport simulations. In Figure 4 we present the isotherms for the case when $a_1^0(P)$ are the Langmuir isotherms, with the coefficients and other data as in Section 2.3.1. Of course, this time the isotherms a_1, a_2 are the IAS derived a_1^{IAS}, a_2^{IAS}.

We notice the difference in the position of the shock for the CO2 component and the shape of rarefaction wave for the CH4 component between the results shown in Figure 3 and Figure 4.

4. Hybrid Porescale Models of Adsorption

The goal of the porescale models discussed here is to derive the relationship(s) $a(u)$ from first principles, and to follow up to get the multicomponent isotherms $a_i^{IAS,MFEQ}$. As we have seen, the relationships such as (15) apply to Darcy scale models, and are not intended to recognize the local pore-scale geometry. When derived experimentally, they reflect average equilibrium behavior of adsorbent interacting with the adsorbate.

In contrast, porescale models can account for detail configurations of adsorbed fluid, and can be built from first principles. In the last two decades, porescale models have been applied to study single and multi-phase dynamics of flow and transport, and they range from traditional PDE models [54, 55], through pore network models, [36, 37, 1, 5], to Lattice Boltzmann (LB) methods [77, 71, 65, 75]. The adsorption models at porescale we consider here fall in the category of lattice gas models and specifically, equilibrium statistical mechanics based on first principles formulations of energy functionals. Other first-principles methods include molecular dynamics (MD) and density functional

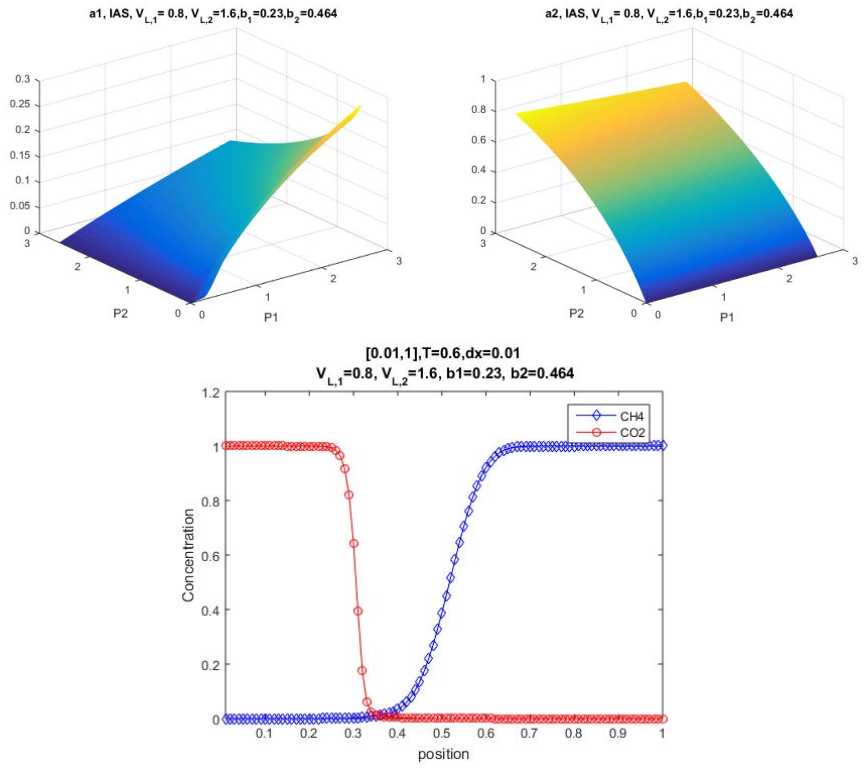

Figure 4. Isotherms and the corresponding transport solution for IAS model. The parameters of the single component Langmuir isotherms a_i^0 are $V_{L,1} = 0.8, b_1 = 0.23, b_2 = 0.464, V_{L,2} = 1.6$, and these are similar to those used for CH4 and CO2, respectively. The remaining data for the simulation are as in Section 2.3.1. Notice the difference between the results shown in Figure 3.

theory (DFT); see [2, 58, 24, 80, 33].

In the context of adsorption phenomena, a significant advantage of the porescale adsorption models considered here is that they can accurately predict hysteresis in adsorption. While we do not address hysteresis explicitly in this paper, this ability is the primary motivation for the study of porescale models.

Hysteresis is a rate independent phenomenon in which the adsorption and desorption proceed along different curves depending on whether the gas pres-

sure P is increasing or decreasing, i.e., on the sign of $\frac{\partial P}{\partial t}$. Hysteresis in multicomponent adsorption is considered significant [79, 23, 29, 61, 66] and in particular for CH4 and CO2 [13, 66, 57] , and there is experimental data published in literature for the primary adsorption and desorption scanning curves. To model hysteresis, one needs to account for reversal of $\frac{dP}{dt}$ at any value of P. The statistical mechanics models can do this.

Statistical mechanics offers an approach in which "deterministic equations describing (large systems of) particles are replaced by assumptions on their statistical behavior" [7]. The model we consider is discrete, i.e., based on an enumerable number of rectangular cells ("sites") ω_i that the solid or fluid particles can occupy. The model is based on a so called *bcc lattice* [33] representation of porescale $\omega = \omega_R \cup \omega_F = \bigcup_{i=1}^{N} \omega_i$. This representation is compatible with binary porescale images obtained from microtomography such as those shown in Figure 1. To understand the connection between the gas reservoir Ω and the porescale region ω, one can consider that at every point x, there is a corresponding porescale geometry $\omega(x)$.

The single component porescale adsorption model described here was introduced in [30] based on [48, 32], and it has been refined and better understood, and compared to other statistical mechanics methods by Monson and his co–authors [29, 78, 79, 64, 44, 60, 62, 60].

We first recall the model, then show how it can be related to the Langmuir model, and then proceed to its analysis in the multicomponent case.

Porescale Geometry

In the model Each site i is occupied either by fluid, or by solid, according to

$$t_i = \begin{cases} 1, & \text{cell is open to fluid} \\ 0, & \text{cell is blocked by solid} \end{cases} \tag{58}$$

$$n_i = \begin{cases} 1, & \text{cell is occupied by fluid} \\ 0, & \text{cell is not occupied by solid} \end{cases} \tag{59}$$

The porescale geometry is therefore denoted by the variable $\mathbf{t}$, the vector of all t_i, and the location of the gas particles is denoted by $\mathbf{n}$, and their local densities are $\rho_i = t_i n_i$. We have $\omega_F := \bigcup_{i:t_i=1} \omega_i$ and we will denote $|\omega_F| := \sum_i t_i$ with the porosity given by $\phi = \frac{|\omega_F|}{|\omega_F|+|\omega_R|} = \frac{N_F}{N}$.

In the model we form the averages over the possible (but stationary) realizations of $\mathbf{n}$. This is in contrast to Lattice Boltzmann or pore network models

where $\mathbf{t}$ is fixed but the fluid particles n_i are transported. We focus on finding equilibrium values of ρ; these depend on the temperature T, i.e., on β, and on the number of particles of adsorbate in the solvent which depends with the chemical potential μ. The variable P is correlated to μ, the chemical potential, which plays the same role as magnetic field in the Ising model.

In the nomenclature of statistical mechanics $\mathbf{t}$ is usually called a (quenched) disorder. Therefore, any simulations we perform should not depend on a particular realization of $\mathbf{t}$, and thus one should average any results over the realizations of disorders $\mathbf{t}$ which share certain common characteristics for a given medium. However, in this paper for simplicity we do not elaborate on this, and consider a fixed geometry $\mathbf{t}$.

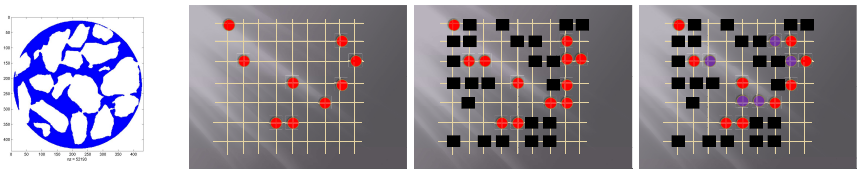

(a) (b) (c) (d)

Figure 5. (a) Example of $\mathbf{t}$ from porescale data, courtesy of the authors of [56, 15], with original resolution $725 \times 725 \times 356$. White pixels denote rock and blue denotes void space. (b-d) Cartoon of lattice gas configurations in free space and in porous medium. Squares indicate locations taken by porous solid and circles indicate locations occupied by gas. (b) Geometry without rock, (c) Single gas component, (d) Multiple gas components.

4.1. Single Component MFEQ Adsorption Model

The interactions of particles with each other and with the porous medium are expressed by a Hamiltonian i.e., an energy functional. Below we provide details; we use traditional notation for $\beta = \frac{1}{k_B T}$ where T is the temperature, and k_B is the Boltzmann constant. The model accounts simultaneously for the combined effects of disorder and confinement, represented by $\mathbf{t}$, and fluid-solid interactions (also known as wetting).

There are two parameters w_{ff}, w_{mf}, denoting the strength of fluid–fluid and matrix-fluid interactions, respectively. The chemical potential μ is related

to the gas pressure, as usual, by

$$\mu = \mu_{ref} + \log\left(\frac{P}{P_{ref}}\right). \tag{60}$$

Hamiltonian for Adsorption

We define now the Hamiltonian $\mathcal{H}$ which accounts for the fluid–fluid and fluid–matrix interactions and for the contact with an external reservoir which provides the source of gas at a given chemical potential μ. We have

$$\mathcal{H} := -\mu \sum_i n_i t_i - w_{ff} \sum_{(i,j)} n_i t_i n_j t_j - w_{mf} \sum_{(i,j)} [n_i t_i (1-t_j) + n_j t_j (1-t_i)], \tag{61}$$

where (i, j) denotes all the nearest neighbor pairs. Here we have followed the notation in [78] which adopts the usual statistical mechanics conventions from [80, 48]. See also similar models, with somewhat different notation in [78, 79, 62, 64]. We refer also to [45, 7, 80] for excellent introduction to the Ising model of magnetisation which is the basic model of statistical mechanics with structure much simpler than that in (61).

In (61) the first term is responsible for the response of fluid cells to the presence of chemical potential μ. With the product $n_i t_i$ we only account for those cells which are not rock-occupied. The second term in (61) favors the aggregation of fluid-only cells, and the third favors the fluid cells in contact with rock.

Realizations of $\mathbf{n}$

Now (61) provides the energy for one realization of the random variable $\mathbf{n}$ selected out of the possible $S = 2^{N_F}$ members of $\Pi := \{\mathbf{n}^{(s)}\}_{s=1}^{S}$. The realizations are also called "states". Of interest to us are some average (macroscopic) quantities such as gas density, or its energy, that can be derived from $\mathbf{n}$. However, we are only interested in those average quantities that correspond to the equilibria, i.e., to those states $\mathbf{n} \in \Pi$ for which $\mathcal{H}(\mathbf{n})$ is at the minimum.

It is clearly impossible to find such minima analytically for an arbitraty $\mathbf{t}$. The complexity of a "brute force" approach in which we enumerate all the states $\mathbf{n} \in \Pi$ is also prohibitively large. In statistical mechanics there are many avenues to overcome this complexity, and they derive from the fact that many of the states in Π are not very likely to be close to an equilibrium. On the other

hand, there may be multiple states corresponding to an equilibrium, at a given T and μ.

For a given state $\mathbf{n}$ and its energy $\mathcal{H}(\mathbf{n})$, the *equilibrium occupation probability* is given by the Boltzmann probability distribution

$$p(\mathbf{n}) = \frac{1}{Z} e^{-\beta \mathcal{H}(\mathbf{n})}, \tag{62}$$

where Z is the normalizing constant called *partition function* so that

$$Z = \sum_{\mathbf{n} \in \Pi} e^{-\beta \mathcal{H}(\mathbf{n})}. \tag{63}$$

Now for any quantity $Q(\mathbf{n})$ we can calculate its expectation $\langle Q \rangle$

$$\langle Q \rangle = \sum_{\mathbf{n} \in \Pi} Q(\mathbf{n}) p(\mathbf{n}). \tag{64}$$

In particular, one can calculate the average density $\langle \rho_i \rangle$ and

$$\langle \rho \rangle = \frac{1}{N_F} \sum_i \langle \rho_i \rangle. \tag{65}$$

To find macroscopic relationships corresponding to the minimum (equilibrium) states, and overcome the complexity discussed below, in this paper we follow the mean-field equilibrium (MFEQ) approximation approach. MFEQ and the alternative, Monte-Carlo simulations, are summarized in [78]. Below we briefly recall MFEQ, since its form will be needed in the analysis.

We refer to a broad discussion of MFEQ approaches for Ising model of magnetization to [80, 10, 72, 48], while Monte-Carlo simulations are well explained in [45, 80].

Mean-Field Approximations

In the mean-field approximation, one modifies (64) to calculate averages of ρ over only the equilibrium states $\mathbf{n} \in \Pi^*$. Each state $\mathbf{n} \in \Pi^*$ has the corresponding collection of densities $\rho^* = (\rho_i^*)_{1 \le i \le N_F}$.

To find the states in Π^*, the authors in [78] first rewrite the model for $\mathcal{H}$ in terms of (spin) variables $s_i = 2n_i - 1$ which resemble the (site diluted) Ising model application, with a random external field (rather than constant term

related to μ). Then, after some algebraic transformations, they derive that every state in Π^* must be a critical point of a certain functional Ψ which combines the Hamiltonian $\mathcal{H}$ along with the entropy function

$$\beta\Psi := \beta\mathcal{H} + \sum_i \psi(\rho_i). \tag{66}$$

Here $\psi(\rho) := \rho ln(\rho) + (1-\rho) ln(1-\rho)$.

Each critical point of Ψ must be a zero of its derivatives. After transformation back to n_i variables, and some algebra, [78] defined the equilibrium densities as the solutions to

$$\rho_i^* = F_i(\beta, \mu; \rho^*) := \frac{t_i}{1 + \exp(-\beta\mu)\exp(-\beta\sum_{j\in i}(w_{ff}\rho_j^* + w_{mf}(1-t_j))}. \tag{67}$$

Now (67) is of fixed point type.

Solving for Equilibria

To find the solutions to (67), we proceed by Picard's iterations, i.e., by successive substitutions, starting with some initial guess $\rho_i^{*,(0)}$. It is well known that such an iteration need not converge, and if it does, that the answer is unique. However, in practice, only infrequently does the iteration fail to complete [32].

We actually should not expect existence of a unique solution due to the form of Ψ which translates into non-contractiveness of F_i. This can be easily seen for a fixed w_{ff} in the trivial case $N = 1 = N_F$, where for high enough T there is only one equilibrium while for low T there are two equilibria, similarly as in the Ising model of phase transitions [48, 80]. For $N_R = N - N_F >> 1$, there are several metastable equilibria [48, 17], and this leads to adsorption/desorption hysteresis.

Literature on MFEQ for Adsorption

The implementations in [79, 78] with $N = O(64^3)$, $10 \leq M \leq 50$, provided scanning curves qualitatively agreeing with those from experiments and from other computations. The authors considered the realizations of morphology Φ generated from Gaussian random fields using the covariance information from experimental data. This work was later favorably compared in [61, 63, 44] to results of other discrete methods including Monte Carlo with Kawasaki and Glauber dynamics, GCMC, and MD with different Lennard-Jones potentials.

See also [29, 78] for discussion of absence of phase transition in macroscale, [49, 18] for support of independent pore theory, [62] for discussion of ink-bottle theories, and [43] for isolated slit pore calculations based on mean field theory. Most successful are approaches which combine the two theories [4].

The mean-field theory in connection with Landau theory has been able to explain several theories of phase transitions and in particular van-der Waals equation of state [80]. In general, the mean field approximation is capable of producing some good qualitative approximations to phase transitions and critical phenomena. In particular, the equation analogous to (67) for average magnetization m in the original Ising model leads via the Taylor expansions, to scaling laws and further to the concepts of universality, and renormalization. The exact solutions in $d = 1, 2$ by Onsager show discrepancies in the scaling, but these decrease if more long-range interactions are included [80].

4.2. Analysis of the MFEQ Adsorption Isotherms

Now we sketch the analysis of the simplified version of (67). For notation convenience we set $J = w_{ff}$ and $\alpha = \frac{w_{mf}}{w_{ff}}$; we also drop the MFEQ superscript *. Recalling (67) we rewrite the vector equation

$$\rho = F(\beta, \mu; \rho) = \frac{t}{1 + exp(-\beta\mu)exp(-\beta J \sum_{(i,j)} \rho_j + \alpha(1 - t_j)}.$$

It is convenient also to recall (60) where we set $\mu_{ref} = 0, P_{ref} = 1$. (The results do not depend on this choice.) We rewrite

$$\rho = F(\beta, P; \rho) = \frac{t}{1 + P^{-\beta} G(\rho)}, \;\; G(\rho) = \exp\left(-\beta J \sum_{(i,j)} \rho_j + \alpha(1 - t_j) \right). \quad (68)$$

It is clear that the solution ρ to (67), if it exists, must be in $[0, 1]$.

Furthermore, we define the single component isotherms

$$a^{MFEQ}(P) = A\rho(P). \quad (69)$$

where A is a scaling constant dependent on the units required in the transport model. For example, it may reflect the maximum volume of adsorbate which can cover the surface of adosrbent.

Now we check when (68) is guaranteed to have a unique solution. To do so, we analyze $\nabla_\rho F(\beta, P; \rho)$. We consider only the simplified case with $N_F = 1$,

and $t = 1$. We notice that $G(\rho) > 0$, $G'(\rho) = -\beta J G(\rho)$, and we find that F is increasing since

$$\frac{\partial}{\partial \rho} F(\beta, P; \rho) = t\beta J \frac{P^{-\beta} G(\rho)}{(1 + P^{-\beta} G(\rho))^2} > 0. \tag{70}$$

Further, to guarantee existence and uniqueness, we check if F is a contraction. To do so, we write the expression for the derivative as a product of two terms

$$t\beta J \frac{P^{-\beta} G(\rho)}{(1 + P^{-\beta} G(\rho))^2} = \left(\frac{P^{-\beta} G(\rho)}{1 + P^{-\beta} G(\rho)} \right) \left(t\beta J \frac{1}{1 + P^{-\beta} G'(\rho)} \right). \tag{71}$$

Now the first term is always less than 1. The contractivity is thus guaranteed if the second term is less than 1 as well. This in turn is true if, e.g., βJ is sufficiently small, and in particular if the temperature is sufficiently large. For temperature lower than a certain critical value, the solution may be nonunique.

A similar qualitative result is well known for the Ising model, where the uniqueness of solutions breaks for small T (or large β). The hysteresis in [78] reported for large β is one consequence of the nonuniqueness of solutions, and it corresponds to multiple metastable minima of the energy functionals.

Behavior of $\rho(P)$

Next we want to verify that ρ is indeed increasing with P so that later we can verify (46). Note however that ρ is defined implicitly as the solution to (67). We differentiate both sides of (68) and solve for $\frac{d\rho}{dP}$ to obtain, after some algebra

$$\frac{d\rho}{dP} \left[1 - t\beta J \frac{P^{-\beta} G(\rho)}{(1 + P^{-\beta} G(\rho))^2} \right] = \frac{t\beta P^{-\beta - 1} G(\rho)}{(1 + P^{-\beta} G(\rho))^2}.$$

To show positivity of $\frac{d\rho}{dP}$ we notice the right hand side is positive, thus it remains to consider if the factor on the left hand side is positive as well. This however reduces to checking if the derivative given in (71) is less than 1 again. Furthermore, if $\frac{d\rho}{dP} > 0$, then by (69), so is $\frac{d}{dP} a^{MFEQ}(P) > 0$.

In summary, while we have not proven it rigorously, we have reasons to expect that the isotherms $a^{MFEQ}(P)$ are increasing functions of P. Further, their values depend on the assumed porescale geometry $\mathbf{t}$, and the coefficients J, and α. It is clear that these may be specific to the particular gas component and type of adsorbent.

4.2.1. Finding Single Component Isotherms $a_i^{0,MFEQ}$

Finally, when considering the multicomponent extension of these models, we can use the single component isotherms derived, e..g, for a particular set of the coefifcients J_i, α_i and record their values as $a_i^{0,MFEQ}$. Now since they satisfy the sufficient conditions of Proposition 3.1, at least as long as β is small enough, we can infer that the MFEQ–derived adsorption system is hyperbolic and that the eigenvalue properties are the same as those discussed for the EL system, so long as β is small enough.

4.3. Results of MFEQ: Single Component Isotherms $a_i^{0,MFEQ}$

In this paper we consider the porescale geometry as given from tomography images, or generated randomly, for a given porosity ϕ. We only consider two-dimensional images. For tomography sample, we use a subimage of that in Figure 1.

We consider three geometries: cleat, tuff, and synthetic (random); see Figure 6. We are unable to work with the original 3D porescale images of the cleats or of the tuff, due to their high (and poor) resolution. The realistic cleat porosity values are much smaller, around 0.1%; see images in Figure 1. However, it is difficult to visualize or illustrate the model concepts at such a small porosity, hence we choose a similar synthetic "cleat" geometry.

For illustration purposes, we scale all images to a 100×100 lattice, and ignore the considerations of the effects of (finite) lattice size. We also create a synthetic image of a cleat, due to the difficulties with the resolution of that in Figure 1. In addition, we select a portion of the tuff data shown in Figure 6 of size 400×400 and subsequently upscale it by a factor 4 in each direction. The porosity in our random "micropore" geometries varies, from 0.1 to 0.5. While one could average over different tomography images, or different random realizations of $\mathbf{t}$, this will not be done here.

Our focus is on the qualitative properties of the isotherms, and we do not make an attempt to correlate the MFEQ adsorption isotherms to the experiments. In simulations below we keep parameter $J = w_{ff} = 1$ fixed, and change only $\alpha = \frac{w_{mf}}{w_{ff}}$. We also vary β.

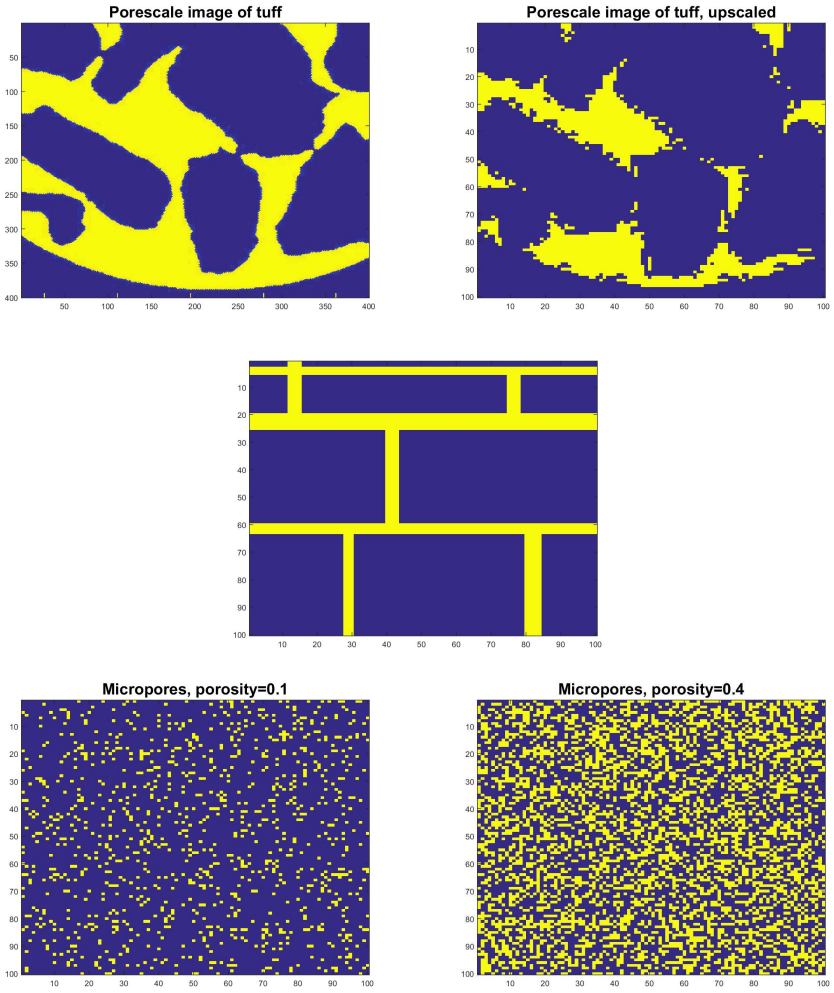

Figure 6. Geometries used in porescale simulations with MFEQ methodology. Top: the "tuff" geometry scaled to 100×100 lattice. Middle: the synthetic "cleat" geometry. Bottom: the "micropore" geometry with $\phi = 0.1$ and $\phi = 0.4$.

4.3.1. Computational Results

In Figure 7 we show the adsorption isotherms derived for the three geometries considered. The MFEQ isotherms derived with the data summarized in

Table 3, and are plotted along with the Langmuir fit. For details of the fit and dependence of the V_L and $b = B_L$ on the coefficient $\alpha = \frac{w_{mf}}{w_{ff}}$, please see Table 3.

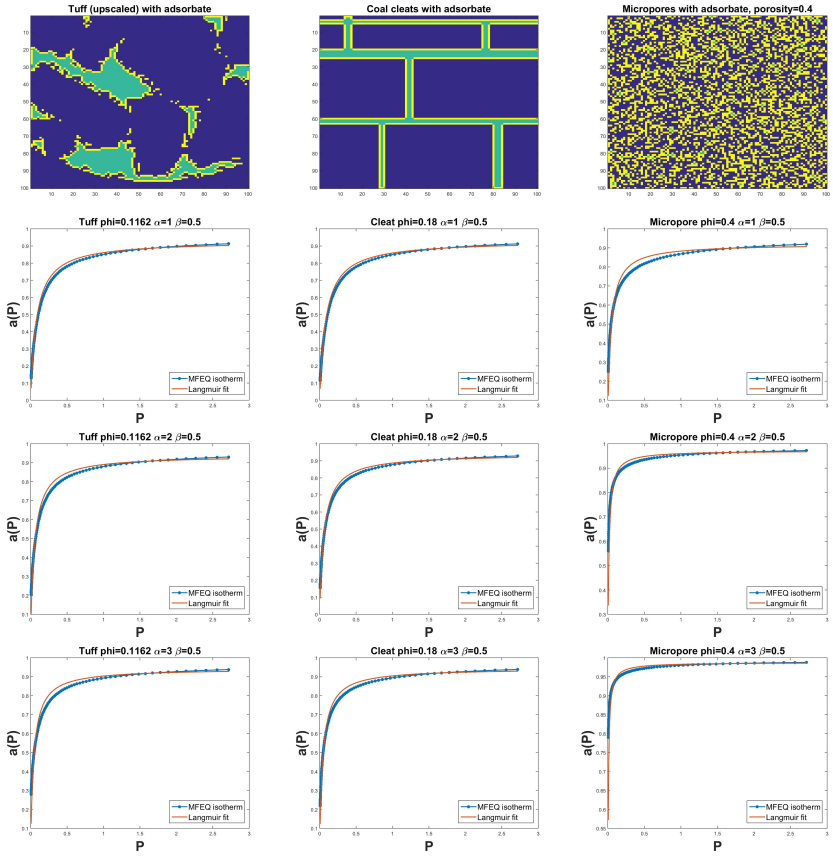

Figure 7. Top: three examples of geometries with the film of adsorbate shown for illustration. Below: the graphs of isotherms corresponding to each geometry for $\beta = 0.5$ and different strength α of fluid/solid interaction. The rows correspond to $\alpha = 1$, $\alpha = 2$, and $\alpha = 3$. Each graphs displays the MFEQ isotherm along with the fit to a Langmuir isotherm.

In Figure 8 we report on the effect of the temperature, or of β. It is clear that as β increases, the Langmuir fit is not adequate, In fact, the slope of $a(p)$

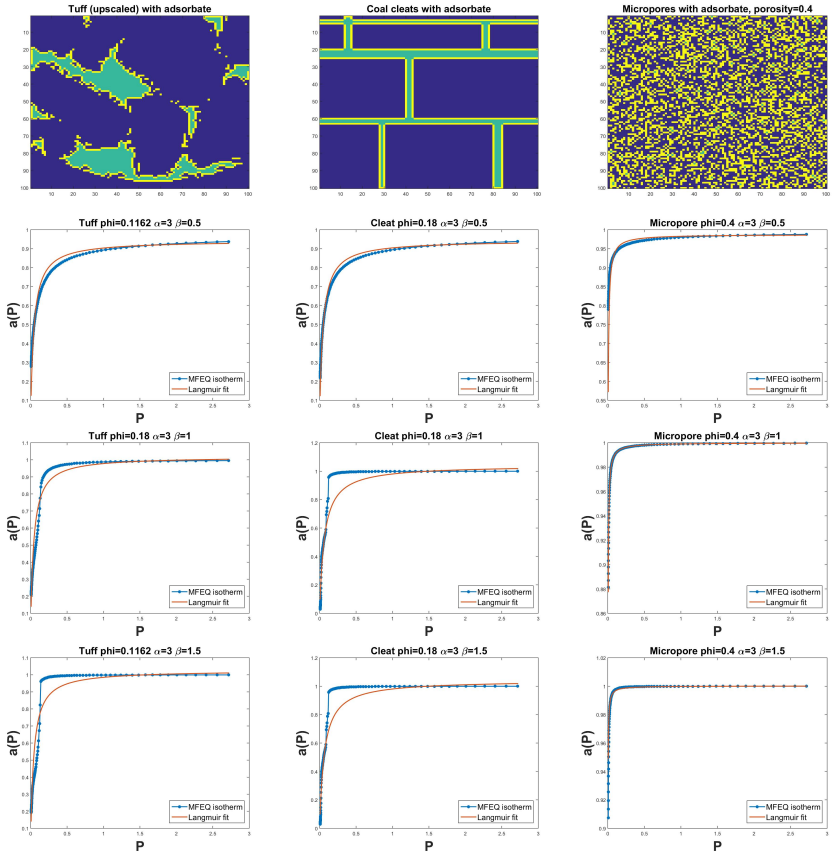

Figure 8. Effect of β on the isotherms for all three geometries. Top, middle, and bottom show the results for $\beta = 0.5, 1, 1.5$, respectviely. All use $\alpha = 3$.

close to 0 increases, and the shape of the isotherm changes.

The coefficient γ for each configuration is the ratio of the amount of density of fluid in the adsorbate layer to the equilibrium density ρ. Of course, γ is proportional to $\frac{N_A}{N_F}$.

The next issue is how the strength w_{mf} of matrix-fluid and w_{ff} of fluid-fluid interactions affects the shape of the isotherms. We study this by changing the ratio $\frac{w_{mf}}{w_{ff}}$. One can see the qualitative difference in Figure 7 between the isotherms corresponding to different α. In addition, in Figure 9 we track the

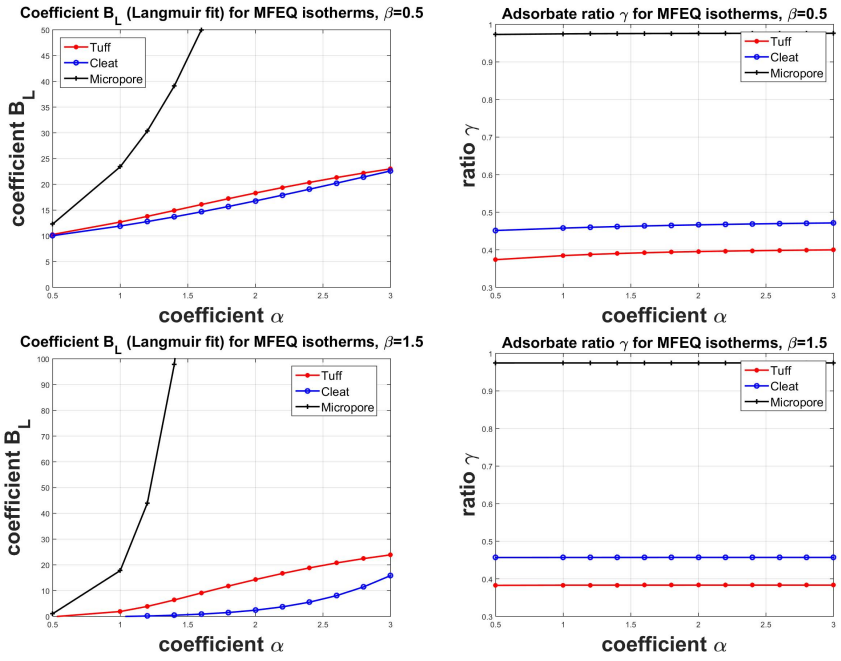

Figure 9. Properties of MFEQ isotherms for the three geometries. Left: the coefficient B_L calculated from Langmuir fit for a given α. Right: ratio γ of adsorbate density with respect to the fluid density for each equilibrium state.

dependence of the fit of B_L from Langmuir model to α, for a fixed temperature $\frac{1}{\beta}$. We also collect selected numeric values in Table 3.

4.3.2. Multicomponent MFEQ Isotherms

One can postulate a multicomponent extension to the single-component theory described in Section 4.1. However, some questions remain as concerns the proper Mean Field Equilibrium formulation, and more research is underway. Possible avenues include extensions similar to the Potts model in order to avoid multiple fluiod occupancy, or a straightforward extension in whch the Hamiltonian penalizes the occupancy by multiple fluids.

Instead, we propose IAS as a proper method to combine multiple isotherms. We fix $J = 1$, and calculate the isotherm $a_1^{0,MFEQ}(P)$ derived for a chosen

Table 3. The ratio $\alpha = \frac{w_{mf}}{w_{ff}}$ of interactions between matrix and fluid and the corresponding B_L in Langmuir fit to the MFEQ isotherms, at high temperature ($\beta = 0.5$) and lower temperature ($\beta = 1.0$). The values of α are selected so that the corresponding B_L are approximately doubled, mimicking the known ration between the B_L values for CH4 and CO2.

Geometry	β	α	B_L	α	B_L
Cleat	0.5	1.0	12.91	3	22.60
Cleat	1.0	1.0	2.66	1.6	5.28
Tuff	0.5	1.0	12.68	3	23.01
Tuff	1.0	1.0	4.81	1.6	11.22
Micropore 0.4	0.5	1	23.416	1.6	49.98
Micropore 0.4	1.0	1	23.7304	1.2	43.01

value of α_1 with the MFEQ algorithm. Next we pick α_2 and calculate the isotherm $a_2^{0,MFEQ}(P)$.

We proceed next within the IAS framework to derive $a_i^{IAS,MFEQ}(P_1, P_2), i = 1, 2$. This step requires numerical integration and the use of lookup tables. Furthermore, once $a_i^{IAS,MFEQ}, i = 1, 2$ are calculated, we proceed to simulate the transport solutions.

Case Studies

We set up two case studies, one dubbed "Data A", and the other "Data B". Both use the "cleat" geometry.

Case **DATA A**. We use $\alpha_1 = 1$, and the Langmuir fit is $V_L = 1$, $B_L = 11.91$. For $\alpha_2 = 3$, the fit is $V_L = 1$, and $B_L = 22.60$.

Case **DATA B**. We use $\alpha_1 = 1$ and $\alpha_2 = 1.6$.

In the case DATA A we use $\beta = 0.5$ and the MFEQ isotherms $a_i^{0,MFEQ}$, have a good Langmuir fit. In the case DATA B $\beta = 1.5$ and the fit is poor; recall the evidence above.

As concerns transport simulations, we can compare these to the results shown in Figure 3 and Figure 4. We notice the difference in the shock spped for the CO2 component and the shape of rarefaction wave for the CH4 component.

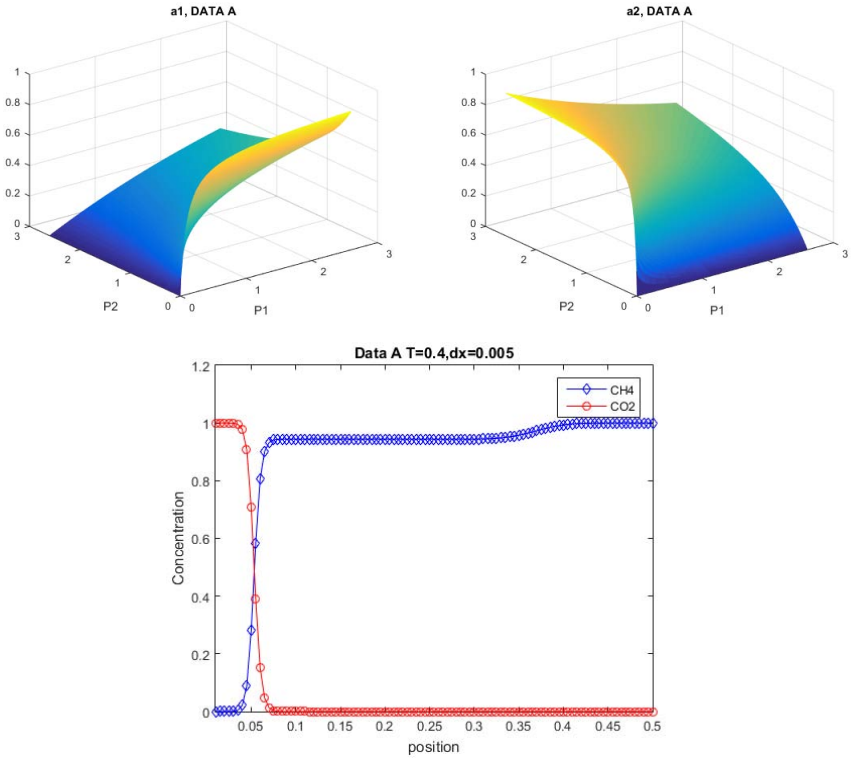

Figure 10. Isotherms and the corresponding transport solution for IAS model which uses MFEQ derived single component isotherms $a_i^{0,MFEQ}$. These are obtained with the simulation parameters for the case "DATA A". The remaining data for the simulation are as in Section 2.3.1, with the exception of dt=0.025.

The results are now put together; see Figures 10 and 11 corresponding to the "Data A" and "Data B" cases. We show the multicomponent isotherms $a_i^{IAS,MFEQ}$ obtained from the single component lookup-data $a_i^{0,MFEQ}$ for each case as well as the corresponding transport results.

These results demonstrate that our approach is viable. More importantly, the comparison between the IAS isotherms for the case "DATA A" (Langmuir-like) and "DATA B" (not Langmuir-like) shows that the hybrid methodology we developed is indeed worth the effort, and not merely an exercise. The isotherms

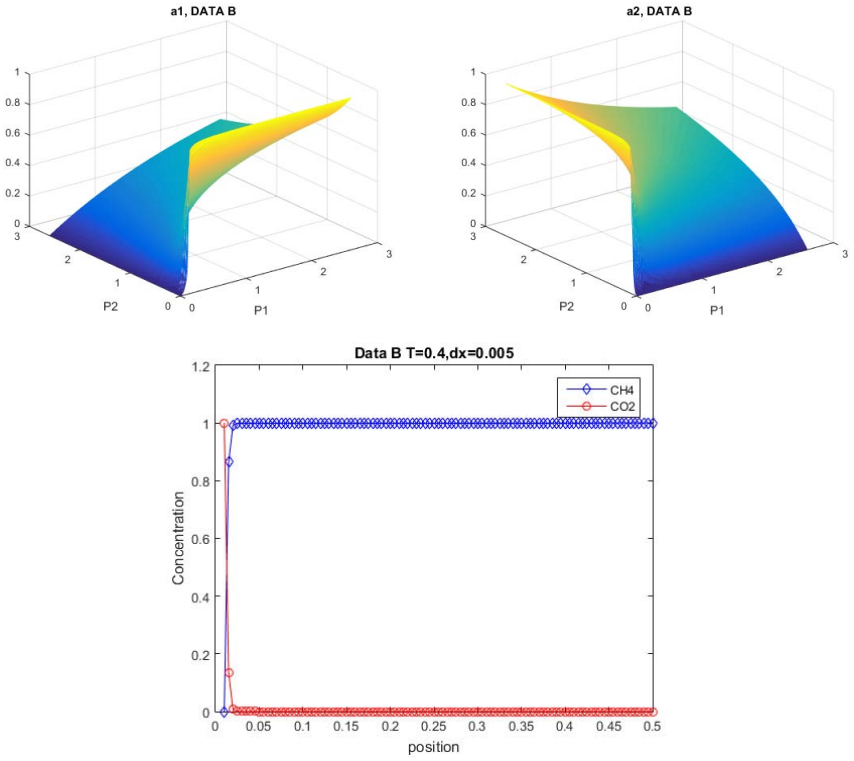

Figure 11. Isotherms and the corresponding transport solution for IAS model which uses MFEQ derived single component isotherms $a_i^{0,MFEQ}$. These are obtained with the simulation parameters for the case "DATA B". The remaining data for the simulation are as in Section 2.3.1, with the exception of dt=0.025.

for DATA B case have qualitative behavior distinct from DATA A or Langmuir cases in that they switch from concave to locally convex. This requires further studies, and in particular, over different geometries $\mathbf{t}$.

5. Conclusion

In this paper we described a hybrid methodology which connects statistical mechanics models, and in particular, the mean field MFEQ approach, to derive

the multicomponent adsorption isotherms. We demonstrate that one can start with a particular porescale geometry and derive single component isotherms which can be next used, within IAS framework, to calculate the corresponding multicomponent isotherms. The methodology works very well, as long as the temperature is not too low, and the solutions to MFEQ problems can be found by iteration. Furthermore, we embed the methodology in the framework of conservation laws, and provide appropriate analysis of hyperbolicity condition and of the appropriate CFL stability constraints.

Future work includes validation, verification, and testing, as well as connecting the MFEQ models to experimental data. More analysis of MFEQ and extensions of the MFEQ model, as well as including local porescale transport and diffusion, are underway.

Acknowledgments

Last but not least we would like to thank several colleagues for sharing their data and expertise. Porescale tuff data was obtained from Dorthe Wildenschild, Oregon State University. Coal samples were obtained from Katarzyna Czerw and Grazyna Ceglarska-Stefanska. The imaging is courtesy of Anna Trykozko and Marek Dohnalik.

We also acknowledge the funding from National Science Foundation, within NSF-DMS 1115827 “Hybrid modeling in porous media” and NSF-DMS 1522734 “Phase transitions in porous media across multiple scales”.

References

[1] David Adalsteinsson and Markus Hilpert. Accurate and efficient implementation of pore-morphology-based drainage modeling in two-dimensional porous media. *Transp. Porous Media*, 65(2):337–358, 2006.

[2] M.P. Allen and D.J. Tildesley. *Computer Simulation of Liquids*. Oxford Science Publishers, 1987.

[3] Todd Arbogast, Jim Douglas, Jr., and Ulrich Hornung. Derivation of the double porosity model of single phase flow via homogenization theory. *SIAM J. Math. Anal.*, 21(4):823–836, 1990.

[4] P. C. Ball and R. Evans. Temperature dependence of gas adsorption on a mesoporous solid: capillary criticality and hysteresis. *Langmuir*, 5(3):714–723, 1989.

[5] Martin Blunt. Flow in porous media pore-network models and multiphase flow. *Current Opinion in Colloid & Interface Science*, 6:197–207, 2001.

[6] Grant S Bromhal, W Neal Sams, Sinisha Jikich, Turgay Ertekin, and Duane H Smith. Simulation of co 2 sequestration in coal beds: The effects of sorption isotherms. *Chemical Geology*, 217(3):201–211, 2005.

[7] Oliver Bühler. *A brief introduction to classical, statistical, and quantum mechanics*, volume 13 of *Courant Lecture Notes in Mathematics*. New York University Courant Institute of Mathematical Sciences, New York, 2006.

[8] Andreas Busch, Yves Gensterblum, Bernhard M. Krooss, and Ralf Littke. Methane and carbon dioxide adsorption-diffusion experiments on coal: upscaling and modeling. *International Journal of Coal Geology*, 60(2-4):151 – 168, 2004.

[9] Andreas Busch, Yves Gensterblum, Bernhard M. Krooss, and Nikolai Siemons. Investigation of high-pressure selective adsorption/desorption behaviour of co2 and CH4 on coals: An experimental study. *International Journal of Coal Geology*, 66(1-2):53 – 68, 2006.

[10] Herbert B. Callen. *Thermodynamics, an introduction to physical theories of equilibrium thermostatics amd irreversible thermodynamics*. Wiley, 1960.

[11] Grazyna Ceglarska-Stefanska and Katarzyna Zarebska. The competitive sorption of CO2 and CH4 with regard to the release of methane from coal. *Fuel Processing Technology*, 77-78:423 – 429, 2002.

[12] Grazyna Ceglarska-Stefanska and Katarzyna Zarebska. Sorption of carbon dioxide-methane mixtures. *International Journal of Coal Geology*, 62(4):211 – 222, 2005.

[13] C. R. Clarkson and R. M. Bustin. The effect of pore structure and gas pressure upon the transport properties of coal: a laboratory and modeling

study. 1. isotherms and pore volume distributions. *Fuel*, 78(11):1333 – 1344, 1999.

[14] L.D. Connell and C. Detournay. Coupled flow and geomechanical processes during enhanced coal seam methane recovery through CO2 sequestration. *International Journal of Coal Geology*, 77(1-2):222 – 233, 2009. CO2 Sequestration in Coals and Enhanced Coalbed Methane Recovery.

[15] K.A. Culligan, D. Wildenschild, B.S.B. Christensen, W.G. Gray, M.L. Rivers, and A.F.B. Tompson. Interfacial area measurements for unsaturated flow through a porous medium. *Water Resources Research*, 40(W12413):1–12, 2004.

[16] Katarzyna Czerw. Methane and carbon dioxide sorption/desorption on bituminous coal–experiments on cubicoid sample cut from the primal coal lump. *International Journal of Coal Geology*, 85(1):72–77, 2011.

[17] Pablo G. Debenedetti. *Metastable liquids. concepts and principles*. Princeton University Press, 1996.

[18] Duong D. Do. *Adsorption analysis: equilibria and kinetics*. Imperial College Press, 1998.

[19] Masaji Fujioka, Shinji Yamaguchi, and Masao Nako. CO2-ECBM field tests in the ishikari coal basin of japan. *International Journal of Coal Geology*, 82(3-4):287 – 298, 2010. Asia Pacific Coalbed Methane Symposium: Selected papers from the 2008 Brisbane symposium on coalbed methane and CO2-enhanced coalbed methane.

[20] Y. Gensterblum, P. van Hemert, P. Billemont, E. Battistutta, A. Busch, B.M. Krooss, G. De Weireld, and K.-H.A.A. Wolf. European interlaboratory comparison of high pressure CO2 sorption isotherms ii: Natural coals. *International Journal of Coal Geology*, 84(2):115 – 124, 2010.

[21] Edwige Godlewski and Pierre-Arnaud Raviart. *Numerical approximation of hyperbolic systems of conservation laws*, volume 118. Springer Science & Business Media, 2013.

[22] A.L. Goodman, A. Busch, R.M. Bustin, L. Chikatamarla, S. Day, G.J. Duffy, J.E. Fitzgerald, K.A.M. Gasem, Y. Gensterblum, C. Hartman,

C. Jing, B.M. Krooss, S. Mohammed, T. Pratt, R.L. Robinson Jr., V. Romanov, R. Sakurovs, K. Schroeder, and C.M. White. Inter-laboratory comparison ii: CO2 isotherms measured on moisture-equilibrated argonne premium coals at 55c and up to 15mpa. *International Journal of Coal Geology*, 72(3-4):153 – 164, 2007.

[23] P.A. Monson H.-J. Woo, L. Sarkisov. Understanding adsorption hysteresis in porous glasses and other mesoporous materials. In *Characterization of porous solids VI ; Studies in surface science and catalysis*, volume 144. 2002.

[24] J. M. Haile. *Molecular Dynamics Simulation*. Wiley, 1997.

[25] Satya Harpalani, Basanta K. Prusty, and Pratik Dutta. Methane/CO2 sorption modeling for coalbed methane production and CO2 sequestration. *Energy & Fuels*, 20(4):1591–1599, 2006.

[26] Ulrich Hornung and Ralph E. Showalter. Diffusion models for fractured media. *J. Math. Anal. Appl.*, 147(1):69–80, 1990.

[27] Kristian Jessen, Wenjuan Lin, and Anthony R. Kovscek. Multicomponent sorption modeling in ECBM displacement calculations. *SPE 110258*, 2007.

[28] Kristian Jessen, G. Tang, and A. R. Kovscek. Laboratory and simulation investigation of enhanced coalbed methane recovery by gas injection. *Transport in Porous Media*, 73:141–159, 2008.

[29] E. Kierlik, P. A. Monson, M. L. Rosinberg, L. Sarkisov, and G. Tarjus. Capillary condensation in disordered porous materials: Hysteresis versus equilibrium behavior. *Phys. Rev. Lett.*, 87(5):055701, Jul 2001.

[30] E. Kierlik, M.L. Rosinberg, G. Tarjus, and E. Pitard. Mean-spherical approximation for a lattice model of a fluid in a disordered matrix. *Molecular Physics: An International Journal at the Interface Between Chemistry and Physics*, 95:341–351, 1998.

[31] G. R. King, T. Ertekin, and F. C. Schwerer. Numerical simulation of the transient behavior of coal-seam degasification wells. *SPE Formation Evaluation*, 2:165–183, April 1986.

[32] David Lancaster, Enzo Marinari, and Giorgio Parisi. Weighted mean-field theory for the random field Ising model. *J. Phys. A*, 28(14):3959–3973, 1995.

[33] D.P. Landau and K. Binder. *A Guide to Monte-Carlo Simulations in Statistical Physics*. Cambridge, 2000.

[34] Randall J. LeVeque. *Numerical methods for conservation laws*. Lectures in Mathematics ETH Zürich. Birkhäuser Verlag, Basel, 1990.

[35] Randall J. LeVeque. *Finite difference methods for ordinary and partial differential equations*. Society for Industrial and Applied Mathematics (SIAM), Philadelphia, PA, 2007. Steady-state and time-dependent problems.

[36] Li Li, Catherine A. Peters, and Michael A. Celia. Upscaling geochemical reaction rates using pore-scale network modeling. *Advances in Water Resources*, 29(9):1351 – 1370, 2006.

[37] W. Brent Lindquist. Network flow model studies and 3D pore structure. In *Fluid flow and transport in porous media: mathematical and numerical treatment (South Hadley, MA, 2001)*, volume 295 of *Contemp. Math.*, pages 355–366. Amer. Math. Soc., Providence, RI, 2002.

[38] Zofia Majewska, Grazyna Ceglarska-Stefanska, Stanislaw Majewski, and Jerzy Zietek. Binary gas sorption/desorption experiments on a bituminous coal: Simultaneous measurements on sorption kinetics, volumetric strain and acoustic emission. *International Journal of Coal Geology*, 77(1-2):90 – 102, 2009. CO2 Sequestration in Coals and Enhanced Coalbed Methane Recovery.

[39] P. Massarotto, S.D. Golding, J.-S. Bae, R. Iyer, and V. Rudolph. Changes in reservoir properties from injection of supercritical CO2 into coal seams – a laboratory study. *International Journal of Coal Geology*, 82(3-4):269 – 279, 2010. Asia Pacific Coalbed Methane Symposium: Selected papers from the 2008 Brisbane symposium on coalbed methane and CO2-enhanced coalbed methane.

[40] S. Mazumder, K. Wolf, P. van Hemert, and A. Busch. Laboratory experiments on environmental friendly means to improve coalbed methane pro-

duction by carbon dioxide/flue gas injection. *Transport in Porous Media*, 75:63–92, 2008. 10.1007/s11242-008-9222-z.

[41] F. P. Medina and M. Peszynska. Stability with new quantity of interest for kinetic systems. in preparation.

[42] F. Patricia Medina. *Mathematical Treatment and Simulation of Methane Hydrates and Adsorption Models*. PhD thesis, Oregon State University, Corvallis, Oregon, 2014.

[43] P. A. Monson. Contact angles, pore condensation, and hysteresis: Insights from a simple molecular model. *Langmuir*, 24(21):12295–12302, 2008. PMID: 18834164.

[44] Peter Monson. Recent progress in molecular modeling of adsorption and hysteresis in mesoporous materials. *Adsorption*, 11:29–35(7), July 2005.

[45] Mark EJ Newman, Gerard T Barkema, and MEJ Newman. *Monte Carlo methods in statistical physics*, volume 13. Clarendon Press Oxford, 1999.

[46] Zhejun Pan and Luke D. Connell. A theoretical model for gas adsorption-induced coal swelling. *International Journal of Coal Geology*, 69(4):243 – 252, 2007.

[47] Zhejun Pan, Luke D. Connell, and Michael Camilleri. Laboratory characterisation of coal reservoir permeability for primary and enhanced coalbed methane recovery. *International Journal of Coal Geology*, 82(3-4):252 – 261, 2010. Asia Pacific Coalbed Methane Symposium: Selected papers from the 2008 Brisbane symposium on coalbed methane and CO2-enhanced coalbed methane.

[48] Giorgio Parisi. *Statistical Field Theory*. Addison-Wesley, 1988.

[49] Roland J.-M. Pellenq, Benoit Coasne, Renaud O. Denoyel, and O. Coussy. Simple phenomenological model for phase transitions in confined geometry. 2. capillary condensation/evaporation in cylindrical mesopores. *Langmuir*, 25(3):1393–1402, 2009.

[50] M. Peszyńska. A differential model of adsorption hysteresis with applications to chromatography. In Jorge Guinez Angel Domingo Rueda, editor,

III Coloquio sobre Ecuaciones Diferenciales Y Aplicaciones, May 1997, volume II. Universidad del Zulia, 1998.

[51] M. Peszynska. Numerical scheme for a conservation law with memory. *Numerical Methods for PDEs*, 30:239–264, January 2014.

[52] M. Peszynska, R. Showalter, and S.-Y Yi. Flow and transport when scales are not separated: Numerical analysis and simulations of micro- and macro-models. *International Journal Numerical Analysis and Modeling*, 12:476–515, 2015.

[53] M. Peszyńska and R. E. Showalter. A transport model with adsorption hysteresis. *Differential Integral Equations*, 11(2):327–340, 1998.

[54] M. Peszynska and A. Trykozko. Pore-to-core simulations of flow with large velocities using continuum models and imaging data. *Computational Geosciences*, 17:623–645, 2013. DOI: 10.1007/s10596-013-9344-4.

[55] M. Peszynska, A. Trykozko, Gabriel Iltis, Steffen Schlueter, and Dorthe Wildenschild. Biofilm growth in porous media at the porescale: modeling and upscaling, paper invited and abstract accepted for the special issue of awr on pore scale modeling and experiments to be submitted by feb. 15, 2015, editors I. Lunati and M. Prodanovic. *Advances in Water Resources*, 2015.

[56] Mark L. Porter, Marcel G. Schaap, and Dorthe Wildenschild. Lattice-Boltzmann simulations of the capillary pressure-saturation-interfacial area relationship for porous media. *Advances in Water Resources*, 32(11):1632 – 1640, 2009.

[57] Basanta Kumar Prusty. Sorption of methane and CO2 for enhanced coalbed methane recovery and carbon dioxide sequestration. *Journal of Natural Gas Chemistry*, 17(1):29 – 38, 2008.

[58] D.C. Rapaport. *The art of molecular dynamics simulation*. Cambridge, 4 edition, 2009.

[59] E. Ruckenstein, A. S. Vaidyanathan, and G.R. Youngquist. Sorption by solids with bidisperse pore structures. *Chemical Engrg. Science*, 26:1305–1318, 1971.

[60] L. Sarkisov and P. A. Monson. Computer simulations of phase equilibrium for a fluid confined in a disordered porous structure. *Phys. Rev. E*, 61(6):7231–7234, Jun 2000.

[61] L. Sarkisov and P. A. Monson. Hysteresis in Monte Carlo and Molecular Dynamics simulations of adsorption in porous materials. *Langmuir*, 16(25):9857–9860, 2000.

[62] L. Sarkisov and P. A. Monson. Modeling of adsorption and desorption in pores of simple geometry using molecular dynamics. *Langmuir*, 17(24):7600–7604, 2001.

[63] L. Sarkisov and P. A. Monson. Molecular dynamics simulation of adsorption in pores of a simple geometry. *Langmuir*, 17, 2001.

[64] L. Sarkisov and P. A. Monson. Lattice model of adsorption in disordered porous materials: Mean-field density functional theory and Monte Carlo simulations. *Physical Review E (Statistical, Nonlinear, and Soft Matter Physics)*, 65(1):011202, 2002.

[65] M.G. Schaap, M.L. Porter, B.S.B. Christensen, and D. Wildenschild. Comparison of pressure-saturation characteristics derived from computed tomography and Lattice Boltzmann simulations. *Water Resour. Res.*, 43(W12S06), 2007.

[66] C. J. Seto, G. T. Tang, K. Jessen, A. R. Kovscek, and F. M. Orr. Adsorption Hysteresis and its Effect on CO2 Sequestration and Enhanced Coalbed Methane Recovery. *AGU Fall Meeting Abstracts*, pages D1542+, December 2006.

[67] J. Q Shi and S. Durucan. A bidisperse pore difussion model for methane displacement desorption in coal by CO_2 injection. *Fuel*, 82(2):1219–1229, 2003.

[68] Ji-Quan Shi, Saikat Mazumder, Karl-Heinz Wolf, and Sevket Durucan. Competitive methane desorption by supercritical CO2; injection in coal. *Transport in Porous Media*, 75:35–54, 2008. 10.1007/s11242-008-9209-9.

[69] J.Q. Shi and S. Durucan. A bidisperse pore diffusion model for methane displacement desorption in coal by CO2 injection. *Fuel*, 82:1219–1229, 2003.

[70] Hema J. Siriwardane, Raj K. Gondle, and Duane H. Smith. Shrinkage and swelling of coal induced by desorption and sorption of fluids: Theoretical model and interpretation of a field project. *International Journal of Coal Geology*, 77(1-2):188 – 202, 2009. CO2 Sequestration in Coals and Enhanced Coalbed Methane Recovery.

[71] Sauro Succi. *The Lattice Boltzmann equation for fluid dynamics and beyond*. Numerical Mathematics and Scientific Computation. The Clarendon Press Oxford University Press, New York, 2001. Oxford Science Publications.

[72] Colin J. Thompson. *Classical Equilibrium Statistical Mechanics*. Oxford Science Publishers, 1988.

[73] Frank van Bergen, Pawel Krzystolik, Niels van Wageningen, Henk Pagnier, Bartlomiej Jura, Jacek Skiba, Pascal Winthaegen, and Zbigniew Kobiela. Production of gas from coal seams in the Upper Silesian Coal Basin in Poland in the post-injection period of an ECBM pilot site. *International Journal of Coal Geology*, 77(1-2):175 – 187, 2009. CO2 Sequestration in Coals and Enhanced Coalbed Methane Recovery.

[74] G.X. Wang, X.R. Wei, K. Wang, P. Massarotto, and V. Rudolph. Sorption-induced swelling/shrinkage and permeability of coal under stressed adsorption/desorption conditions. *International Journal of Coal Geology*, 83(1):46 – 54, 2010.

[75] D. Wildenschild, K.A. Culligan, and B.S.B. Christensen. Application of x-ray microtomography to environmental fluid flow problems. In U. Bonse, editor, *Developments in X-Ray Tomography IV*, volume 5535 of *Proc. of SPIE*, pages 432–441. SPIE, Bellingham, WA, 2004.

[76] Karl-Heinz A.A. Wolf, Frank van Bergen, Rudy Ephraim, and Henk Pagnier. Determination of the cleat angle distribution of the RECOPOL coal seams, using CT-scans and image analysis on drilling cuttings and coal blocks. *International Journal of Coal Geology*, 73(3-4):259 – 272, 2008.

[77] Dieter A. Wolf-Gladrow. *Lattice-Gas cellular automata and Lattice Boltzmann models*. Lecture Notes in Mathematics 1725. Springer, 2000.

[78] Hyung-June Woo and P. A. Monson. Phase behavior and dynamics of fluids in mesoporous glasses. *Phys. Rev. E*, 67(4):041207, Apr 2003.

[79] Hyung-June Woo, L. Sarkisov, and P. A. Monson. Mean-field theory of fluid adsorption in a porous glass. *Langmuir*, 17(24):7472–7475, 2001.

[80] J.M. Yeomans. *Statistical Mechanics of Phase Transitions*. Oxford, 1992.

[81] Hongguan Yu, Guangzhu Zhou, Weitang Fan, and Jianping Ye. Predicted CO2 enhanced coalbed methane recovery and CO2 sequestration in china. *International Journal of Coal Geology*, 71(2-3):345 – 357, 2007.

[82] Hongguan Yu, Lili Zhou, Weijia Guo, Jiulong Cheng, and Qianting Hu. Predictions of the adsorption equilibrium of methane/carbon dioxide binary gas on coals using Langmuir and Ideal Adsorbed Solution theory under feed gas conditions. *International Journal of Coal Geology*, 73(2):115 – 129, 2008.

[83] Katarzyna Zarebska and Grazyna Ceglarska-Stefanska. The change in effective stress associated with swelling during carbon dioxide sequestration on natural gas recovery. *International Journal of Coal Geology*, 74(3-4):167 – 174, 2008.

About the Authors

F. Patricia Medina was born in Caracas, Venezuela. She received her Bachelor's degree in Mathematics from Universidad Central de Venezuela, Caracas, Venezuela, in 2001. She also received two Masters degrees in Mathematics; one in "Universidad de los Andes", Merida, Venezuela, in 2003 (with a Scholarship from the Ministry of Science and Technology from Venezuela), and the other at Bowling Green State University, Bowling Green Ohio, in 2003. She received her PhD in Mathematics from Oregon State University in 2014.

In 2004, she joined the department of Mathematics in "Universidad Simon Bolivar", Caracas, Venezuela, as a Lecturer, and in 2006 she became Assistant Professor. After finishing her PhD, she joined the Department of Mathematics in Oregon State University as an Instructor. In Summer 2016 she is joining

Worcester Polytechnic institute as a Postdoctoral Fellow. Her current research includes numerical analysis and mathematical and computational treatment of partial differential equations linked to adsorption, methane hydrates and carbon sequestration models. In the past she also worked on non-parametric statistics and Banach space theory, in particular, Orlicz spaces.

Malgorzata Peszynska was born in Warsaw, Poland, in 1962. She obtained her MS degree in Applied Mathematics from Warsaw University of Technology (1986), and her PHD in Mathematics from University of Augsburg in 1992 where she was a DAAD Fellow. She received a Habilitation degree from Warsaw University of Technology in 2011.

She held various visiting and permanent Assisatnt Professor positions at the Polish Academy of Sciences (1986-2003), Warsaw University of Technology (1993-1995), Purdue University (1993-1995), and the University of Texas at Austin (1995-2003), where she worked as Research Associate at the Center for Subsurface Modeling, Institute of Computational Engineering and Science. Since 2003 she has been at Oregon State University as Assistant, Associate, and Full Professor (since 2012).

She is a Fulbright Research Fellow (2009-10), recipient of Stefan Batory travel award (1993), and served as Program Director and Chair of SIAM (Society for Industrial and Applied Mathematics) Activity Group on Geosciences (2008-2012); in 2016-18 she is serving as Vice-Chair of SIAM Pacific Northwest section. She serves on Editorial Board of several journals and has refereed articles for over 30 journals.

Since her PhD she has worked on models of flow and transport using mathematical and numerical analysis as well as computer simulations to understand these phenomena better across various time and spatial scales. She is involved in a variety of interdisciplinary projects with academic, national lab, and industry collaborators from hydrology, oceanography, statistics, environmental, civil and coastal engineering, physics, and materials science, and her research projects were funded by National Science Foundation, and by Department of Energy. She has authored over 50 journal and other refereed publications, and authored over 20 other publications and reports.